

Sensor and Simulation Notes

Note 494

October 2004

## **An Ultra-Compact Impulse Radiating Antenna**

Leland H. Bowen and Everett G. Farr  
Farr Research, Inc.

Dean I. Lawry  
Air Force Research Laboratory / DE

J. Scott Tyo  
University of New Mexico

### **Abstract:**

We describe the development of an Ultra-Compact Impulse Radiating Antenna (UCIRA) intended for space applications in low earth orbit. Because an UWB antenna was desired for this application, an IRA was selected as the starting point for this development. The standard IRA configuration has a single linear polarization and has a very narrow beamwidth at high frequencies. A dual polarization antenna was desired with a larger beamwidth, so we modified the existing design to support dual polarization and we used a hyperbolic reflector to increase the beamwidth. The antenna also had to survive the harsh space environment, be lightweight and very compact for launch, and be remotely deployable.

A deployable IRA with dual polarization using a flexible twinline feed has been developed which has very good RF characteristics. Also, the theory for IRAs with hyperbolic reflectors and defocused feeds has been advanced. The UCIRA-2 developed here met many of the requirements.

## CONTENTS

	<b>Page</b>
1. Introduction.....	3
2. UCIRA-1 Design. ....	5
3. UCIRA-1, RF Measurements.....	8
4. UCIRA-1B, RF Measurements. ....	11
5. UCIRA-2 Design. ....	14
6. UCIRA-2, RF Measurements in Single-Polarity Configuration.....	20
7. UCIRA-2, RF Measurements in Dual Polarity Configuration.....	24
8. UCIRA-2, Environmental Tests.....	29
9. Conclusions and Recommendations .....	32
Appendix A. Defocusing a Paraboloid into a Hyperboloid.....	33
References.....	37

## 1. Introduction.

We summarize here our efforts to build an Ultra-Compact Impulse Radiating Antenna (UCIRA) for space applications. This may be considered an extension of our earlier work to develop an IRA for space applications fabricated from an inflatable membrane [1]. We subsequently decided that the inflatable technology was only appropriate for very large antennas. For the smaller antennas in which we were interested, a mechanically deployable antenna would be more durable. An example of such an antenna is the commercially available CIRA-2 [2], with a diameter of 1.22 m (48 in.). However, the stowed size of the CIRA-2 was too large for satellite applications. This led to the development of the Ultra-Compact IRA or UCIRA, which is described here.

The UCIRA differs from the CIRA-2 in five respects. First, we reduced the collapsed length from 81 cm (32 in.) in the CIRA to 48 cm (19 in.). This was accomplished by reducing the  $F/D$  (focal length / diameter) ratio from 0.4 to 0.3, and by adding a folding joint to each of the 12 radial support rods in the reflector. Second, we defocused the beam with a hyperboloidal reflector, so we could see a larger field of view from Low Earth Orbit (LEO). Third, we configured the antenna to operate with dual polarity. Fourth, we made the antenna automatically deployable with springs and electro-mechanical elements. Fifth, we used materials that could qualify for space applications.

The UCIRA is intended to provide as wide a coverage area as possible from a satellite platform in Low Earth Orbit. In order to receive signals from horizon to horizon, the antenna needs to have a beamwidth of  $100^\circ$  to  $120^\circ$ . Since IRAs are inherently highly directional (narrow beamwidth) at high frequencies, the UCIRA must be defocused using a hyperboloidal reflector instead of a parabolic reflector as described in [3, 4] and Appendix A. We also wanted the bandwidth to be very broad, and a design based on an IRA is well suited for this due to its approximately 2 decades of bandwidth. The CIRA-2, on which the UCIRA is based, is usable from 150 MHz to 10 GHz [5]. In addition, we wanted the antenna to have dual polarity, so twice the information is available from a single antenna.

It has been noted previously by Carl Baum [6] that a hyperboloidal reflector with a circular rim may have a problem in its radiated frequency spectrum on boresight. This occurs at the frequency where the difference in ray path lengths from the center and edge of the reflector is half a wavelength. To address this problem, he proposed using a taper in the reflector shape near the edge of the reflector. Our reflector did not use this, because it was not possible to build our fabric hyperboloid with sufficient accuracy for the problem to become apparent. Besides this, our rim has the shape of a 12-sided polygon, instead of a circle.

The environment in LEO is extremely harsh, so we investigated materials that would stand up to the thermal and radiation environment of space. The thermal cycling in LEO is especially severe and can produce drastic thermal gradients within the antenna structure. The temperature range for the environmental test was  $-60^\circ\text{C}$  to  $+70^\circ\text{C}$ . For the initial version of the antenna the life expectancy desired is one year. Later versions must be able to function for 5 – 10 years. Due to the short life expectancy of the initial version, deterioration due to atomic oxygen and damage due to micrometeoroids were deemed to be negligible.

To study dual polarity IRAs, we experimented with a 46 cm (18 in.) diameter solid aluminum IRA which had two feeds, one for each polarity, vertical and horizontal. This antenna was the IRA-1D. The results of this dual polarity experiment were reported previously in [7].

The first version of the UCIRA (UCIRA-1) was based on the CIRA-2, but it had a number of changes to make it more compact and automatically deployable. The design of this antenna is described in Section 2 and the results of the RF measurements are given in Section 3. This antenna was then modified in hopes of improving its electrical characteristics. The new version was the UCIRA-1B. This antenna, which had exclusion zones in the reflector where the E field has the wrong polarity, is described in Section 4. Both versions of the UCIRA-1 had focused parabolic reflectors, and the feed arms were located at  $\pm 30^\circ$  from the vertical, so they did not have dual polarity capability. Instead, they were optimized for high signal strength on boresight.

The design of the UCIRA-2 is described in Section 5. Although considerable materials research was performed, in most cases the materials used in the UCIRA-2 were similar to those used in previous versions. However, there were several important exceptions. The Ni/Cu plated polyester fabric used for the reflector on the CIRA-2 and UCIRA-1 was replaced with Ni/Ag plated rip-stop nylon. The nickel-over-silver plating maintains its conductivity much better than the nickel-over-copper plating. The aluminum parts were plated with Tufam® to harden the surface and reduce friction where required. Also, the nitrogen-filled gas spring was replaced with standard stainless steel springs, because gas springs lose their pressure at temperatures below  $-40^\circ\text{C}$ . One of the major improvements was the replacement of the manually operated release pin with electrically operated release devices to provide remote activation of the deployment mechanism. A pin puller and an Ejector Release Mechanism (ERM) are used for the two-step deployment of the UCIRA-2.

In Sections 6 and 7 we provide the results of the RF measurements made on the UCIRA-2 in two different configurations. First we tested the antenna in the standard single-polarity mode and then we tested it in the dual polarity mode.

The UCIRA-2 also underwent environmental testing in a Thermal Vacuum chamber (TVac) at the Aerospace Environment Facility (AEF) located on Kirtland AFB. We describe the results of those tests in Section 8.

We begin now with the design of the UCIRA-1.

## 2. UCIRA-1 Design.

We began the UCIRA design with a design concept that was more complicated than necessary. This concept had a telescoping center support tube and bi-fold or Z-fold stays. The bi-fold stays required having part of the deployment mechanism in front of the reflector where it could obstruct the aperture. If the components were non-conductive this obstruction would be minimal. However, we decided that the hinges would have to be metal and the rods would have to be made from a carbon composite material that is rather highly conductive. This led us to seek a new design that removes all obstructions except the feed arms from the aperture.

We then simplified the UCIRA design by a number of methods. By using a single hinge point in the stays and changing the  $F/D$  ratio from 0.4 to 0.3 we were able to fold the IRA down to a length less than the required 0.483 m (19 in.). Changing the  $F/D$  ratio eliminated the need for a telescoping center support rod. These two changes not only reduce the length but simplify the design and thereby improve the reliability of deployment.

In Figure 2.1 we show the UCIRA-1 in the collapsed or stowed configuration on the left. The main body of the collapsed antenna is just under 48 cm (19 in.) long and 18 cm (7 in.) in diameter. An aluminum ring is used to hold the tips of the stays in place. This ring, shown in Figure 2.2, does not work very well and is not used on later versions.

We show the UCIRA-1 in the fully open position on the right in Figure 2.1. The diameter of the reflector is 1.22 m (48 inches). The feed arms for this version have the outer edge inline with the rim of the dish (non-floppy) and are at the more optimum  $\pm 30^\circ$  from the vertical [5, 8, 9, 10, 11] so this version cannot be used in dual polarity mode. The feed arms were accidentally sewn slightly long so there is a problem keeping the feed arms tight. Part of the problem is, also, the very small diameter stays that were used for weight reduction and the higher than expected force required to open the antenna. The next size larger carbon composite rods will be used in the future to provide more stiffness to better support the reflector. A larger gas spring ( $\sim 1.26$  kN) could be used to provide the extra force required by the stiffer stays.

In Figure 2.2 (left) the splitter balun can be seen attached to the side of the can that houses the deployment mechanism. The splitter connects the  $50\ \Omega$  input to two  $100\ \Omega$  cables in parallel. The ends of these cables are connected in series to provide the  $200\ \Omega$  feed for the twinline. The twinline is made from two strands of 26 AWG Teflon insulated wire. To increase the spacing of the conductors, the insulation from 18 AWG wire was placed over the 26 AWG wire. The computed impedance of this combination is  $186\ \Omega$ , which is almost exactly what we measured from the TDR of the cable. The twinline passes through a hole in the reflector and connects to the feed arms at the focus of the parabola. The twinline is approximately 0.56 m (22 in.) long and can be seen in Figure 2.2 as well as on the right in Figure 2.1. The attenuation of the balun/twinline combination is shown in Figure 2.3. The attenuation is below 6 dB out to 10 GHz.

The deployment mechanism is shown on the right in Figure 2.2. The antenna is deployed by pulling the pin (opposite the balun) to release the cam. The cam is pushed forward by a high pressure gas spring (nitrogen filled cylinder). Small levers attached to the ends of the stays are

rotated by the cam to open the reflector. The gas spring not only provides enough force to move the cam, but provides the force required to hold the reflector open. A damper is used to slow the cam so that the stays open at a rate that will not cause damage to the antenna. The damper operates by controlling the flow of air from the inside of the deployment mechanism. The flow is controlled using a needle valve in the back surface of the mechanism. This type of damper cannot be used in space and is replaced with a crushable medium in later versions of the antenna. The Acme-threaded shaft that protrudes through the back of the can is used to retract the cam and compress the high pressure gas spring. This shaft will be omitted on the space version of the antenna.

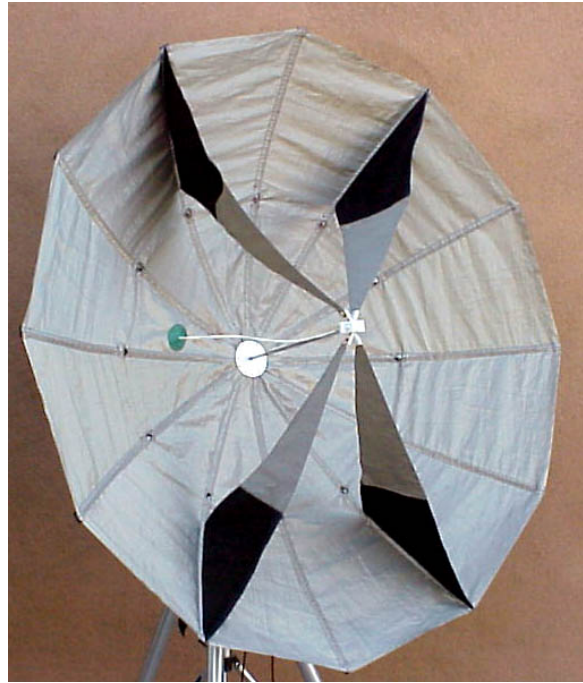


**Figure 2.1 UCIRA-1 in stowed (left) and deployed (right) configurations.**

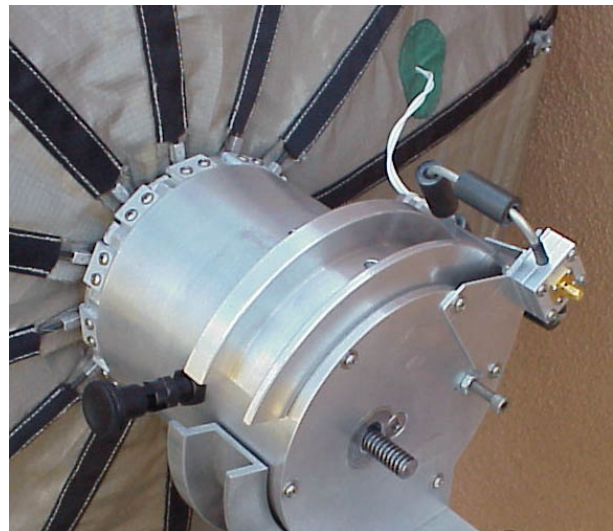
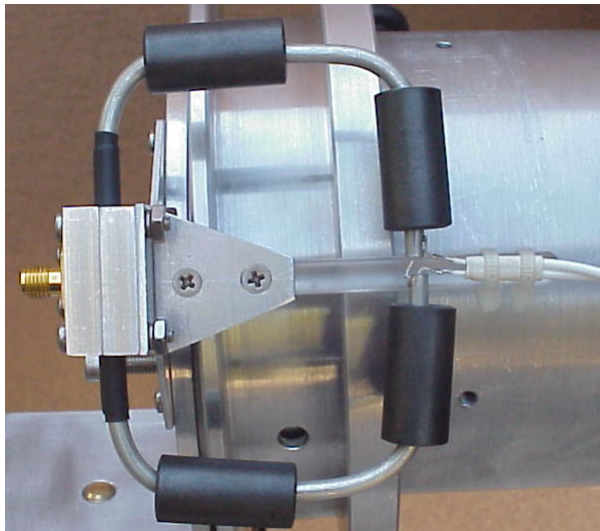


**Figure 2.2 Splitter/Balun (left) and deployment mechanism (right).**

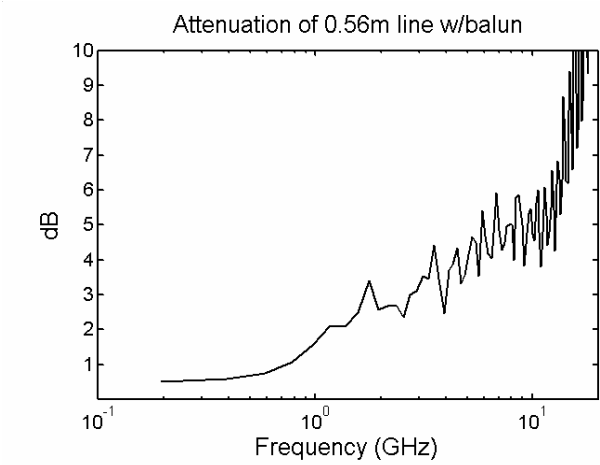


**Figure 2.3 Attenuation of twinline and balun.**

### 3. UCIRA-1, RF Measurements.

We now present the antenna measurements for the UCIRA-1 made at 20 m. The TDR of the UCIRA-1 is presented in Figure 3.1. In Figure 3.2 we see that the impulse response has a FWHM of 67 ps, which is better than we expected, since it is 6 ps better than the commercial CIRA-2. The CIRA-2 has a standard feed with two coaxial cables that extend to the feed point, whereas the UCIRA-1 has a twinline feed that we expected would be less efficient and more lossy at high frequencies. The CIRA-2 is similar to the UCIRA but it has an  $F/D$  of 0.4 instead of 0.3. Thus, we conclude that the twinline feed works much better than we expected.

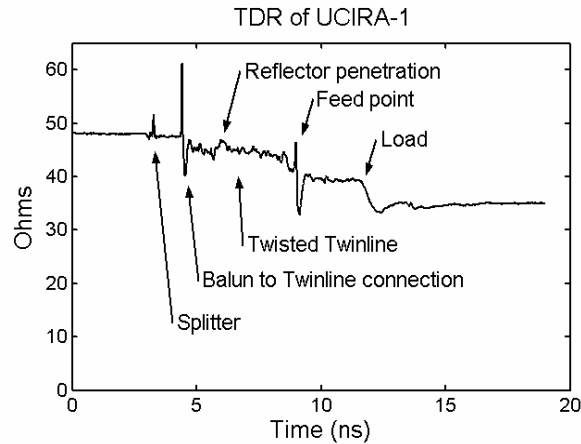


**Figure 3.1 TDR of the UCIRA-1.**

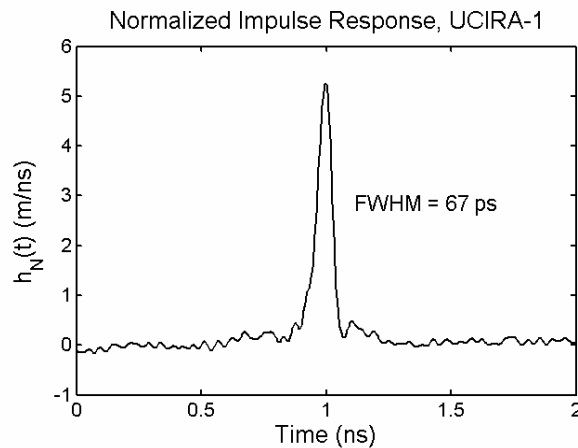


**Figure 3.2 Normalized impulse response.**

In Figure 3.3 we show the realized gain of the antenna with both linear and logarithmic frequency axes. The CIRA-2 data is included in the figure for comparison. We see that the realized gains for the two antennas are about the same up to 10 GHz. The losses due to the twisted twinline are almost negligible. In Figure 3.4 we show the theoretical gain for the UCIRA based on work by J. Scott Tyo [3, 4]. The three lines correspond to defocus parameters  $\phi_0 = 0^\circ$ ,  $1.5^\circ$ , and  $10^\circ$  (see Appendix A). Since the UCIRA-1 has a parabolic reflector, it corresponds to the top line,  $\phi_0 = 0^\circ$ . The measured gain for the UCIRA-1 is considerably lower than the

theoretical value. This is due in part to the dispersion of the reflector, since the reflector is made from 12 panels and therefore is not a true paraboloid of revolution. It is interesting to note the reduction in the gain when a hyperbolic reflector is used to increase the beamwidth.

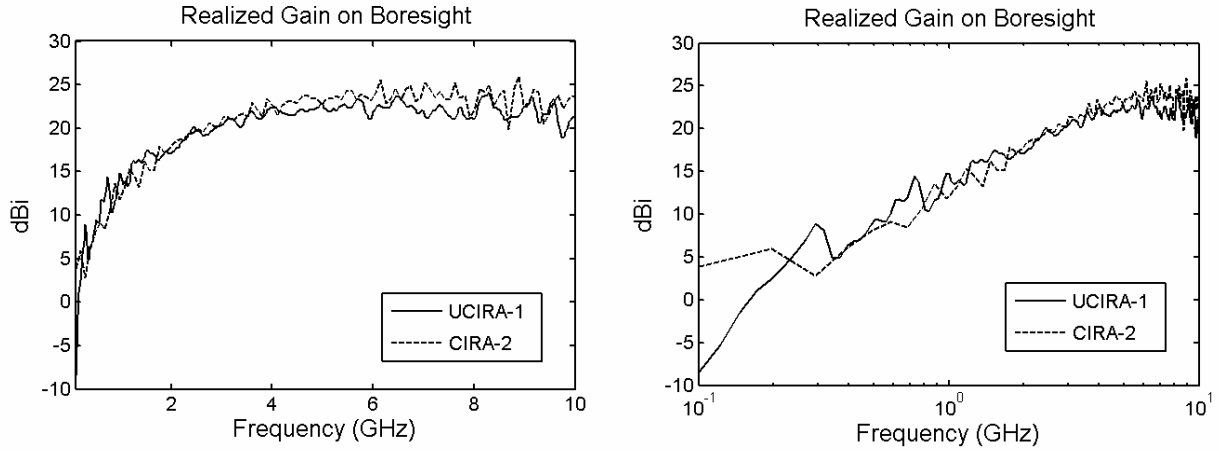


**Figure 3.3 Realized gain of the UCIRA-1 and CIRA-2.**

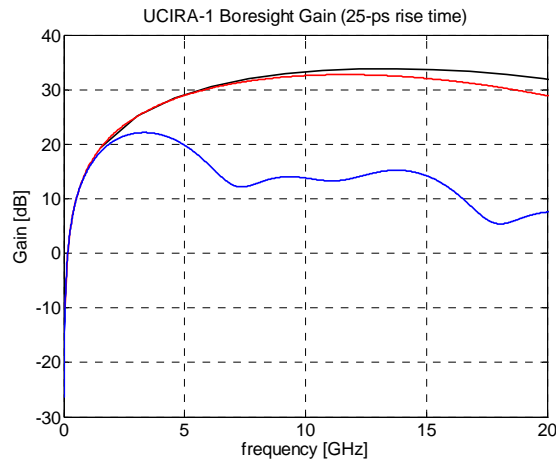


**Figure 3.4 Theoretical gain of UCIRA-1 for defocus parameters of  $\phi_0 = 0^\circ$ ,  $1.5^\circ$ , and  $10^\circ$ .**

In Figure 3.5 we plot the realized gain of the UCIRA-1 for both the copol and crosspol cases. The average crosspol rejection is approximately 20 dB. The antenna patterns on the H and E planes are shown in Figure 3.6. Some sidelobes are evident as is characteristic of the narrow beamwidth of an IRA, although it has been shown that the side lobes are reduced when the feed arms are located at the more optimal  $\pm 30^\circ$  from vertical [12].

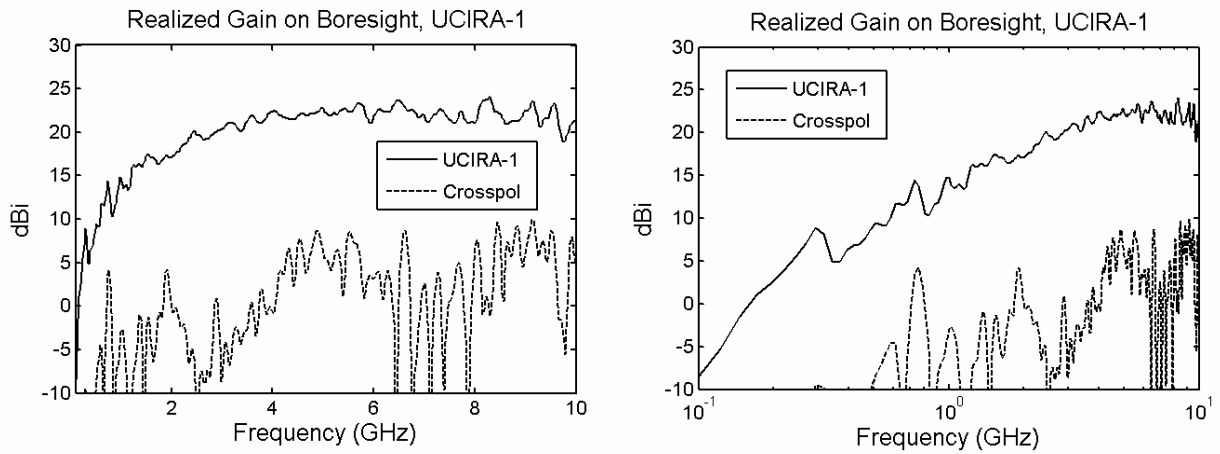


**Figure 3.5 Realized gain of the UCIRA-1 in copol and crosspol.**

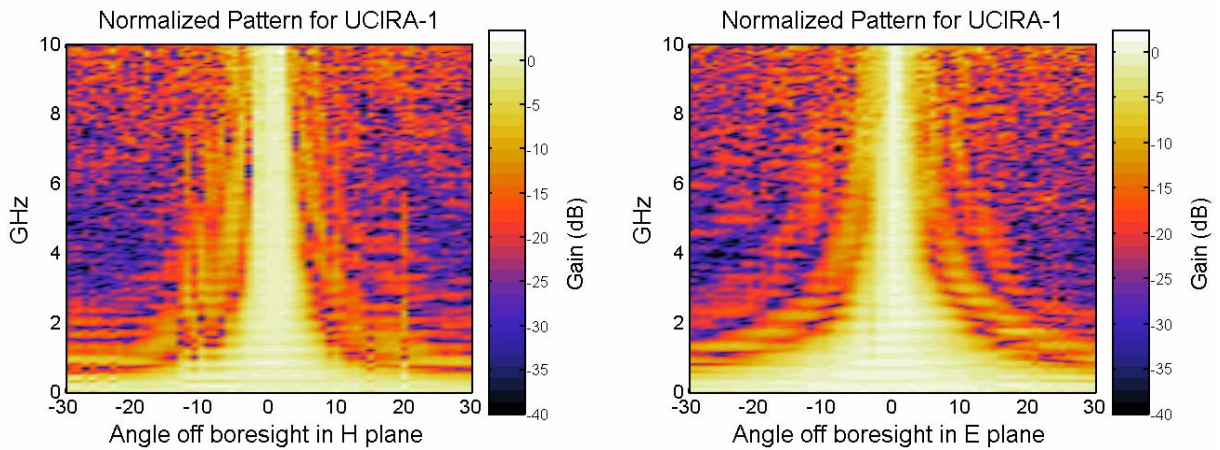


**Figure 3.6 Normalized antenna pattern of the UCIRA-1 in the H and E planes.**

#### 4. UCIRA-1B, RF Measurements.

To get the best possible results from the UCIRA-1, we enhanced it by inserting non-conductive areas into the reflector where the electric field has the wrong polarity [13, 14]. The fields reflected from this area add destructively to the total field, so we expected that allowing these fields to pass through the reflector would increase the overall field strength of the antenna. The non-conductive fabric can be seen in Figure 4.1 between the dark colored resistive sections of the feed arms. We had planned to use this antenna as the standard against which to compare future versions of the UCIRA. However, as can be seen from the data shown below, this antenna did not quite live up to our expectations.



**Figure 4.1 UCIRA-1B.**

For the UCIRA-1B we used the same frame, deployment mechanism, and RF feed components as were used on the UCIRA-1. We modified the shape of the reflector slightly in an attempt to better match the desired paraboloid. Also, the 12 panels were made slightly narrower near the center to eliminate some looseness in the conductive fabric in that region.

In Figure 4.2 we show the TDR of the UCIRA-1B. Overall the TDR of the UCIRA-1B appears to be better than that of the UCIRA-1. The TDR of the splitter is not quite as good as before, even though it is the same splitter, but the balun-to-twinline connection is considerably better. Normally we find that improving the TDR improves the overall performance of the antenna. In this case, however, we see that the normalized impulse response as shown in Figure 4.3 is not as good. The peak is lower, the FWHM greater, and the pulse shape is not as good. These problems are probably due in part to the shape of the reflector which may cause the feed point to be displaced from the focal point of the reflector [4].

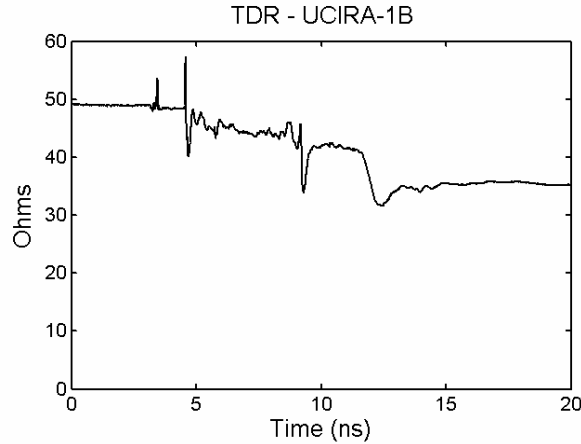


**Figure 4.2 TDR of the UCIRA-1B.**

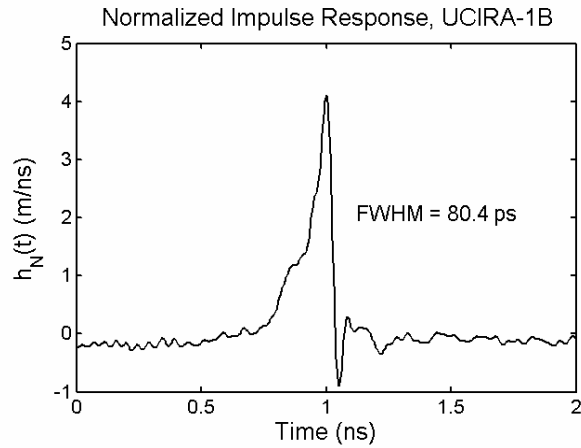


**Figure 4.3 Normalized impulse response.**

In Figure 4.4 and Figure 4.5 we show the realized gain, and antenna pattern for the UCIRA-1B. In Figure 4.4 we have included the realized gain of the UCIRA-1 for direct comparison. The gains of the two antennas are quite similar over much of the frequency range. However, the gain for the UCIRA-1B is considerably lower from 2 to 6 GHz. We have not yet determined a reason for the gain to be low in this region. Since we used the same RF components as were used on the UCIRA-1, the only changes in the feed were slight changes at the balun/twinline interface and at the feed point. The feed point was rebuilt several times in an effort to improve the characteristics of the antenna, but only modest improvements in the TDR and impulse response were achieved. The cross polarization rejection is similar for the two antennas. Cross polarization rejection is not a critical need for this antenna. In Figure 4.5 we see that the beamwidth is somewhat wider in the H or horizontal plan than in the E or vertical plane.

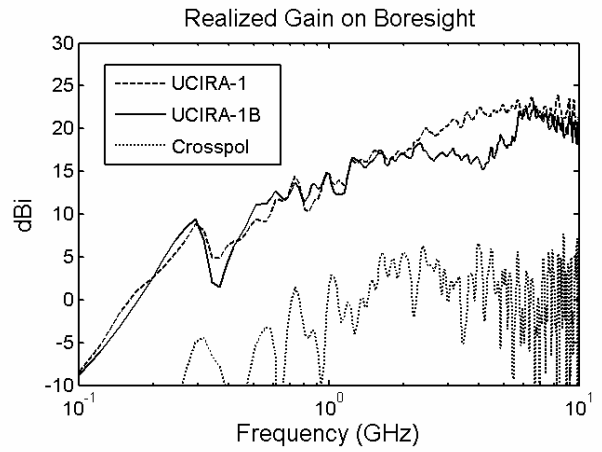
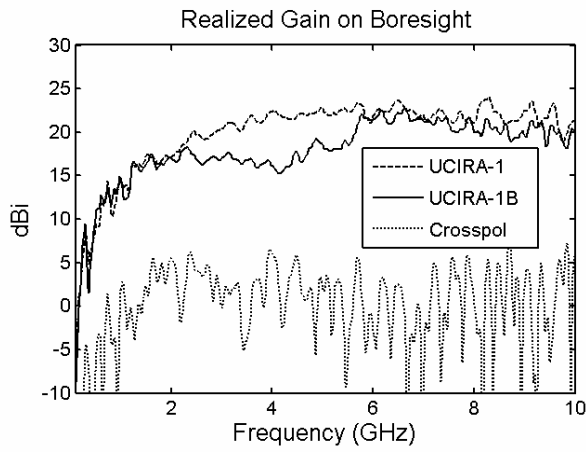


**Figure 4.4 Realized gain on boresight for the UCIRA-1 and 1B.**

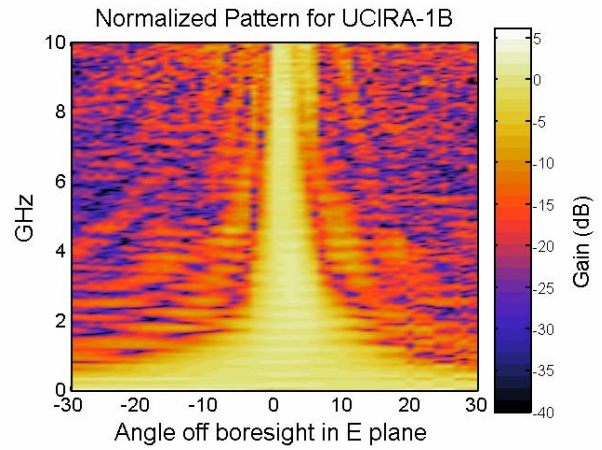
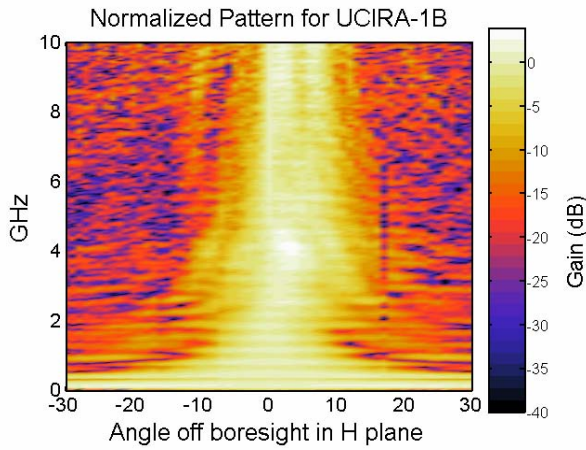


**Figure 4.5 Normalized pattern in the H and E planes for the UCIRA-1B.**

## 5. UCIRA-2 Design.

The design of the UCIRA required considerable research into materials suitable for use in a LEO space environment. The harsh space environment includes long duration vacuum, particle radiation, solar radiation (UV), temperature extremes, rapid thermal cycling, atomic oxygen, and micrometeoroid impact. We gained considerable information on materials and deployable device design from [15]. In the past we have used aluminum and stainless steel for most of the mechanical parts, carbon composite or fiberglass rods for the stays, Ni/Cu plated rip-stop nylon for the feed arms and reflector, and polypyrrole treated polyester for the load resistors. Although we used some of the same or similar materials on the UCIRA-2, there were a number of improvements based on our research and thermal testing.

The Ni/Cu plated nylon fabric used on the UCIRA-1 was replaced with another rip-stop nylon (94EN) that is Ni/Ag plated that does not lose conductivity when creased. We have some concern about the use of nylon in space; however, it appears to work better than expected so we used this material for the UCIRA-2. We also continued to use the polypyrrole treated polyester for the load resistors as we have done in the past. This material has a surface resistance of approximately  $200 \Omega/\text{sq}$  so it is easy to obtain the correct load resistance.

For the ribs or stays that support the reflector we used graphite reinforced composite rods. The hinges in the stays are aluminum with stainless steel torsion springs.

The UCIRA-2 is shown in Figure 5.1 in the stowed and deployed configurations. It has a hyperboloidal reflector to broaden the beamwidth and has dual polarization capability. The hyperboloidal shape should increase the beamwidth by about  $20^\circ$  [4]. The diameter of the reflector is 1.22 m (48 inches) and the F/D is 0.3 as with the UCIRA-1 and 1B. The feed arms have the outer edge inline with the rim of the dish (non-floppy) and are evenly spaced around the reflector to facilitate the dual-polarized feed. The antenna weighs approximately 2.6 kg (5.75 lb.). Most of the mass is in the deployment mechanism. This mass could be reduced somewhat by additional mechanical analysis and reducing the thickness of parts where possible.



**Figure 5.1 UCIRA-2 in stowed (left) and deployed (right) configurations.**

We revisited several issues concerning the mechanical deployment system used on the UCIRA-1 and have made several changes. First we found that the manual release pin on the UCIRA-1 was much too difficult to pull. An automatic pin puller capable of holding the cam in place during launch and then releasing the cam on command was out of the question. Therefore, we replaced the release pin with an Ejector Release Mechanism (ERM) from TiNi Aerospace, Inc. This device is shown in Figure 5.2. Release is accomplished on command (9 VDC at 5 A for 20 ms), by retracting the detent balls that hold the coupler to the actuator, thereby ejecting the coupler as shown on the right in Figure 5.2.

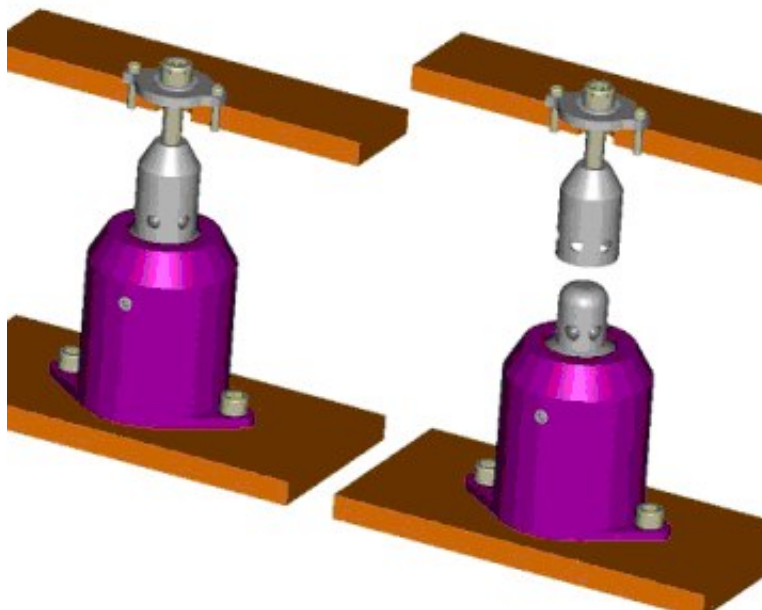


**Figure 5.2 Ejector Release Mechanism (ERM).**

Next, we replaced the gas spring used in the UCIRA-1 with 9 stainless steel conventional springs arranged in a circle around the ERM. The gas spring had the advantage of small size and nearly constant force over the length of the stroke. However, we learned that gas springs cannot be used below  $-40^{\circ}\text{C}$  because they tend to lose the high pressure nitrogen charge at such low temperatures. The 9 conventional springs have a total force of 2.67 kN (600 lb.) in the compressed or launch configuration and 1.33 kN (300 lb.) in the deployed configuration. This provides sufficient force to fully open the reflector with the recommended safety factor [15]. At one point in the development we had planned to use a small servo motor to deploy the reflector; however, these motors are normally custom designed for a particular application, so no adequate off-the-shelf motor was found. An additional problem is that a small motor would require a gear-type speed reducer with a very high mechanical advantage to provide the force required to hold the reflector open. Springs seemed to be the best alternative for the present design but since the antenna opens much faster than we would like, a motor drive may still be required in the future. One problem with the motor drive is that power is needed to drive the motor. This adds weight and/or complexity to the system. The Ti/Ni actuators can be triggered with a 9 V battery.

In Figure 5.3 we show a cross sectional view of the deployment mechanism in the stowed or launch configuration. The stop pin assemblies keep the cam from rotating and lock the cam in the forward position after deployment. The mechanism is shown in the deployed configuration in Figure 5.4. Since we decided to use springs rather than a much more costly and complex motor system, we were forced to include a damping system. This system uses an aluminum honeycomb material, which is crushed to control the opening velocity of the cam and the sudden stop and consequent vibration at the end of the cam's travel. The annular cavity for the honeycomb damping material is shown in Figure 5.3 and Figure 5.4.

The stay adaptor or pivots that position the reflector ribs are shown on the left in Figure 5.3 and Figure 5.4. The pivots are wider at the tip than they are near the pivot points, because the pivots slide on the surface of the cam near the tip. This is done to allow the pivots to contact the cam at the rim, where they are positioned initially, even though there is a slot in the cam at these locations. The slots make it possible for the cam to pass around the narrower section of the pivots, so it can move as far forward as required to fully deploy the reflector. The surfaces of the moving aluminum parts are coated with Tufram® by General Magnaplate. This coating creates a steel-hard, dry-lubricated surface on aluminum that reduces abrasion and corrosion and resists wear and galling. The dry-lubricated surfaces greatly reduce the force required to overcome friction between the various surfaces.

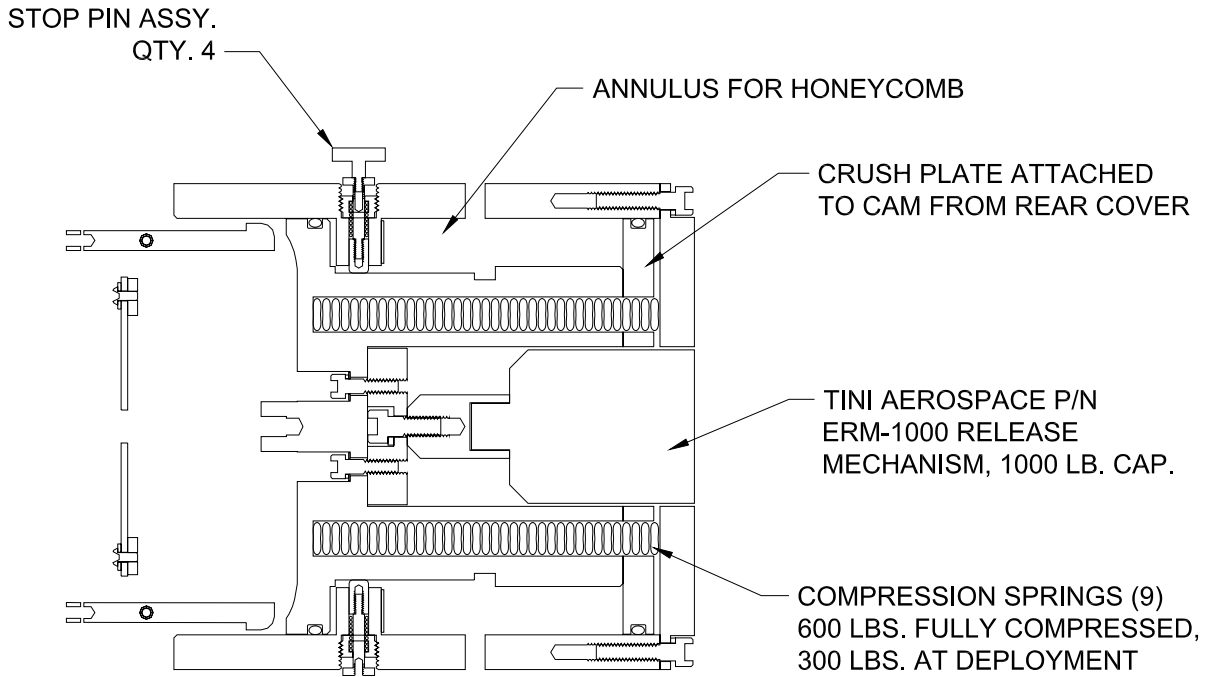


**Figure 5.3 Deployment mechanism in stowed or launch configuration.**

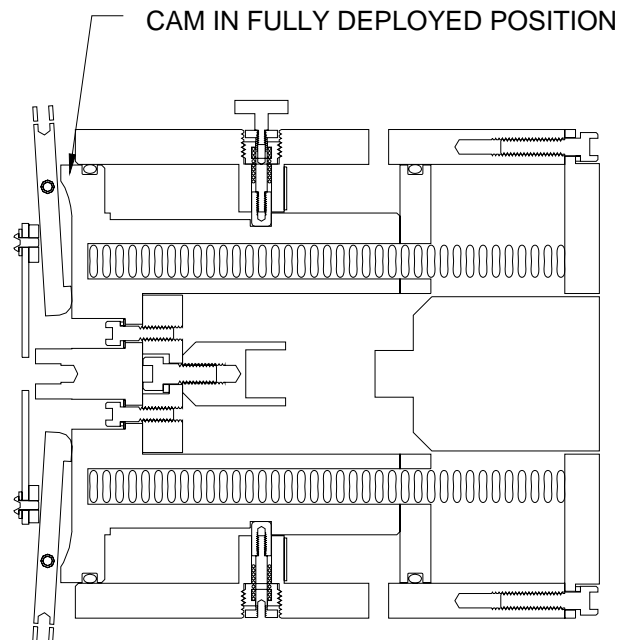


**Figure 5.4 Deployment mechanism in the fully deployed configuration.**

The back side of the deployment mechanism is shown in Figure 5.5. The actuator ERM is located in the center of the back plate and restrains the cam in the stowed configuration. The four (4) holes around the ERM are for the device that compresses the springs to put the UCIRA-2 in stowed configuration. Four rods thread into the back side of the cam through these holes to pull the cam back against the back plate while the coupler on the ERM is attached to hold the cam in place. The pin puller is located to the right and holds the end of a strap that restrains the reflector stays in the stowed configuration. Figure 5.5 also shows the two splitter/baluns (left and top) required for the dual polarity operation of the antenna.

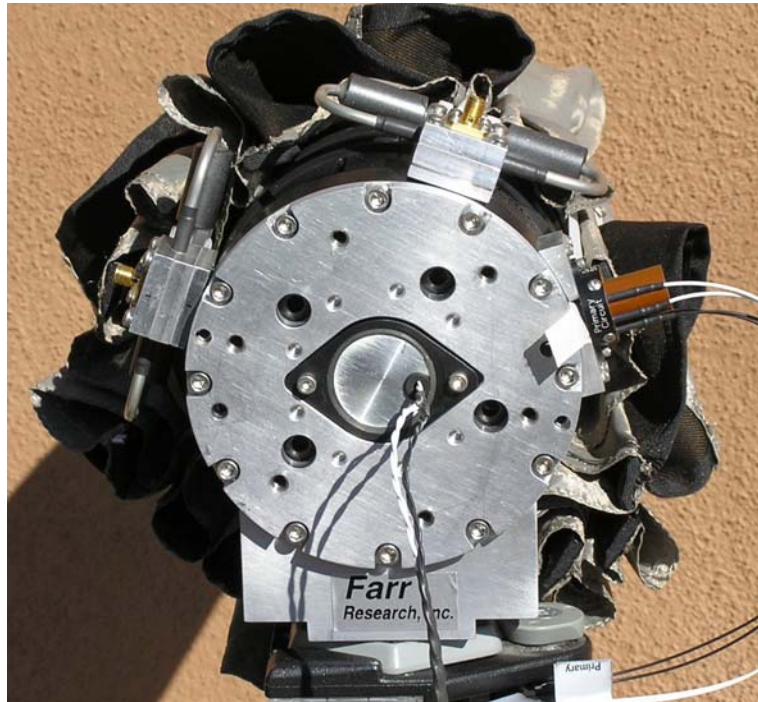


**Figure 5.5 UCIRA-2 deployment mechanism (rear).**

For proper deployment of the UCIRA we had to determine the correct amount of crushable honeycomb material to use to retard the cam, which opens the reflector. We first tried a full circular section of the material and found that the cam was stopped immediately by the honeycomb. After several experiments we found that two sections of a little over 1/8 circle each would allow the reflector to open fully. During these experiments the stay adapters were damaged and had to be replaced. The original stay adapters were made of aluminum and had a very thin cross section at the pivot point. The new stay adapters were made of stainless steel and had a more substantial cross section at the pivot point. The ends of the stay adapters were highly polished to reduce friction where they slide on the front of the cam.

It was found during the deployment tests that the bending moment at the end of the stay adapters tends to over-stress the ends of the stays and several were broken during the tests. Longer stay adapters with deeper holes to support the ends of the stays would reduce this problem and improve the shape of the reflector.

The UCIRA-2 was successfully deployed several times while being video recorded digitally. Pictures taken from the video showing the antenna in the stowed, partially open, and fully deployed states are shown in Figure 5.6. In the first picture the strap that holds the upper section of the stays in the folded position is shown (white). The end of this strap is retained by the pin puller, which is activated first in the deployment sequence. Releasing the strap allows the springs in the stay hinges to partially open the reflector as seen in the second picture. In this photo we see that the right side of the reflector did not open as fully as the left side. However, this did not interfere with the full deployment of the antenna as shown in the third picture. The rim was not as level or even as we would like after this experiment so several slightly damaged stays were replaced before the RF testing described in the next two sections. Also, the interface between the resistive and conductive sections was re-sewn on each of the four feed arms to improve the electrical connection between these sections.

As mentioned earlier, a honeycomb material is used to retard the action of the cam in an attempt to control the speed at which the antenna opens. However, the small sections (about 1/8 circle each) that are required to allow the reflector to open fully also allow the antenna to open very fast. This rapid deployment may produce such a dynamic stress on a space vehicle as to cause problems with the stabilization and orientation system.

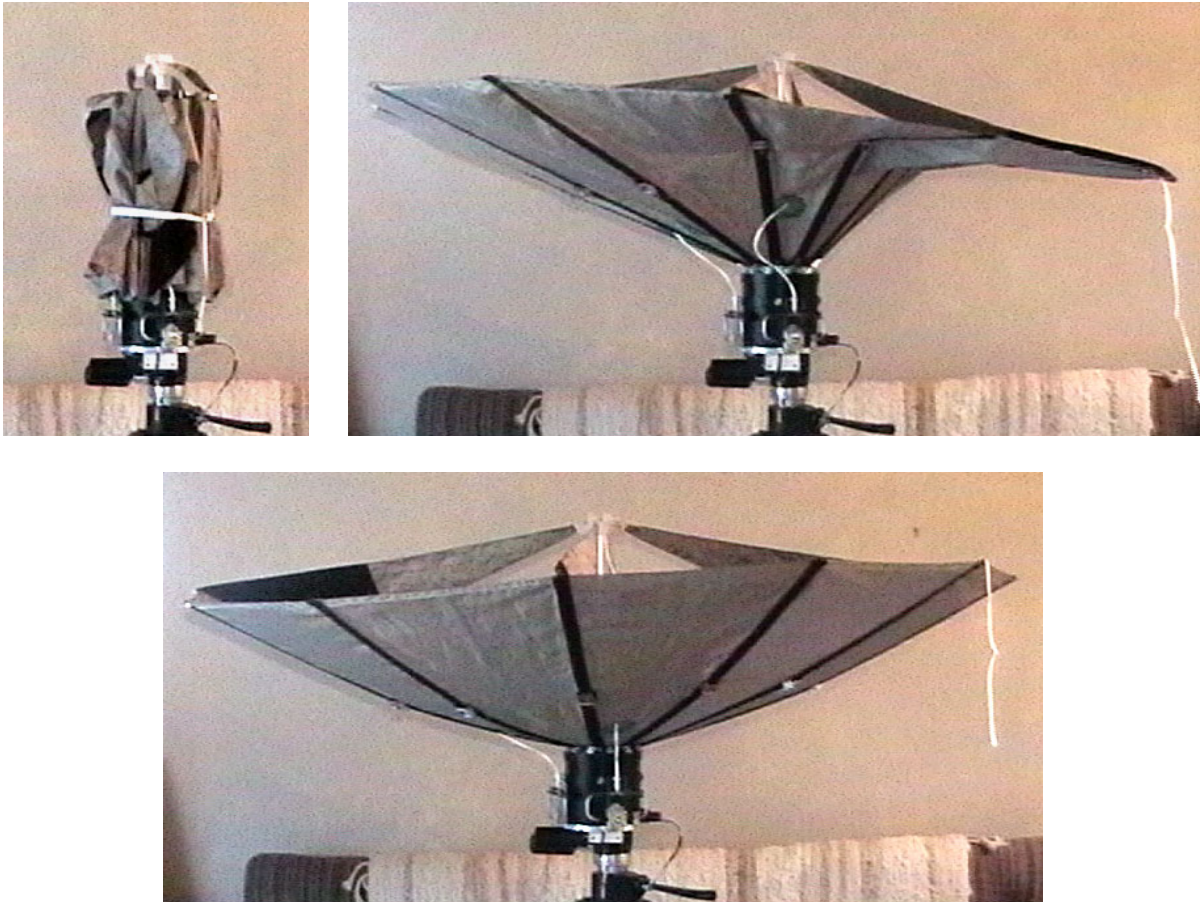


**Figure 5.6 UCIRA-2 in stowed, partially open, and fully deployed configurations.**

## 6. UCIRA-2, RF Measurements in Single-Polarity Configuration.

The RF measurements were made using our newly developed Portable Automated Time-domain Antenna Range (*PATAR*<sup>TM</sup>) System. The system includes a fast pulser, a fast digital sampling oscilloscope, two calibrated TEM field sensors, an elevation/azimuth antenna positioner, a computer controller, and software for system control, data acquisition, and data processing. The fast pulser is a PSPL 4015C with a rise time of approximately 20 ps. The pulser drives one of the TEM sensors to form the transmit portion of the antenna range. The oscilloscope is a Tektronix TDS8000 with a 80E01 sampling head. The UCIRA-2 is connected to the TDS8000 to form the receive section of the system. The UCIRA-2 is shown in Figure 6.1 mounted on the *PATAR*<sup>TM</sup> antenna positioner. The antenna positioner has a non-conductive mast that supports the UCIRA-2 at approximately 3 m above the ground. The distance between the apertures was 20 m.



Figure 6.1 RF testing of UCIRA-2 using *PATAR*<sup>TM</sup> system.

The TDR of the UCIRA-2 in the standard (single-polarity) IRA configuration is shown in Figure 6.2. The various parts of the feed are shown in the figure. The discontinuity at the balun/twinline interface is greater than we would like and it may be possible to improve this interface.

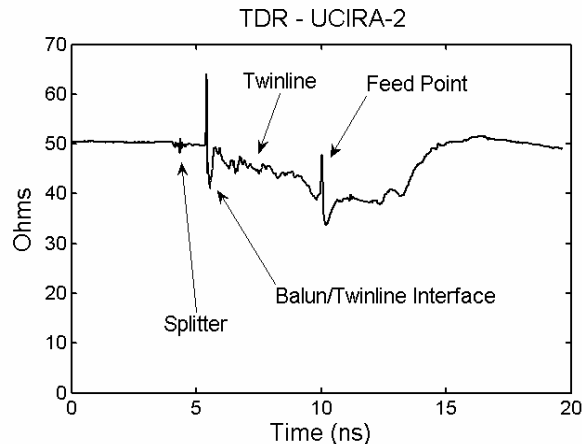


**Figure 6.2 TDR of the UCIRA-2 in standard IRA configuration.**

We show the normalized impulse response in Figure 6.3. The impulse response has a reasonable shape, but the FWHM is greater than we would like. This reduces the gain at high frequencies. The depth of the reflector varies about 4 cm from one side to the other which is not desirable. This is due in part to repairs that had to be made to the feed arms. The required overlap of 1 cm between the conductive and resistive sections of the feed arms was not maintained as accurately as we would like so the overall length of the feed arms varies a little.

In Figure 6.4 we show the realized gain as a function of frequency for the UCIRA-2 in copol and crosspol. The gain shown in Figure 6.4 rolls off some between 4 GHz and 10 GHz but the peak gain is comparable to that of the UCIRA-1 and 1B. For comparison, we provide in Figure 6.5 the gain of the CIRA-2, which is significantly better between 5 and 10 GHz, because its reflector is a paraboloid instead of a hyperboloid.

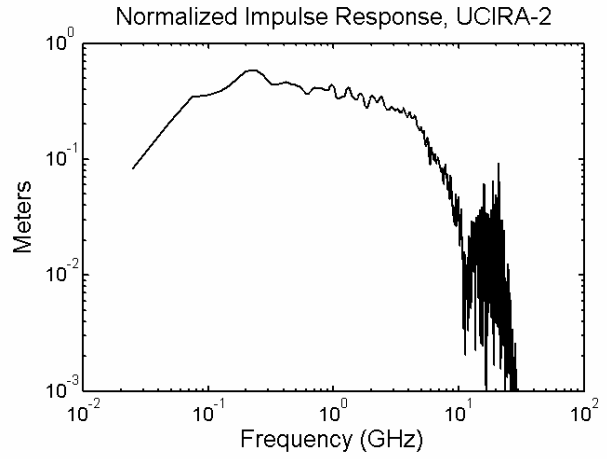
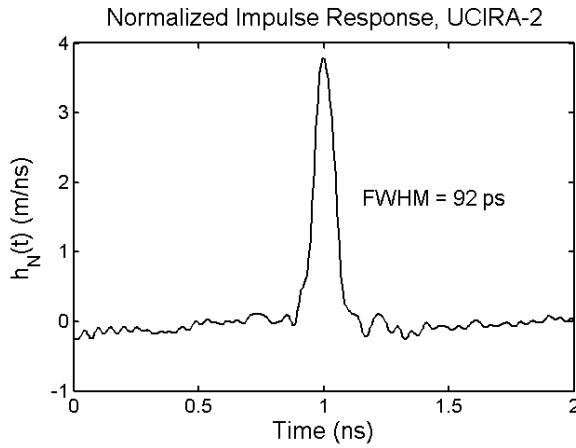


**Figure 6.3 Normalized impulse response of the UCIRA-2.**

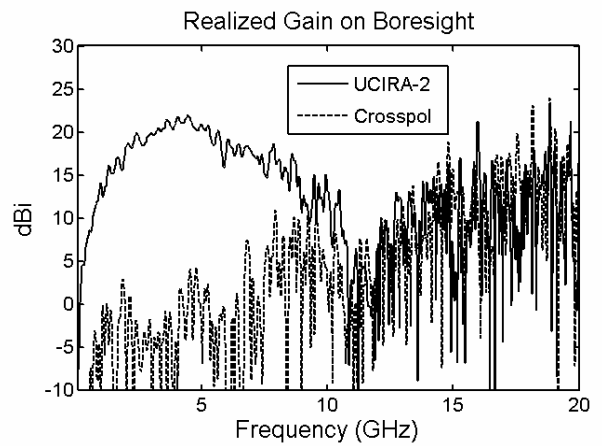
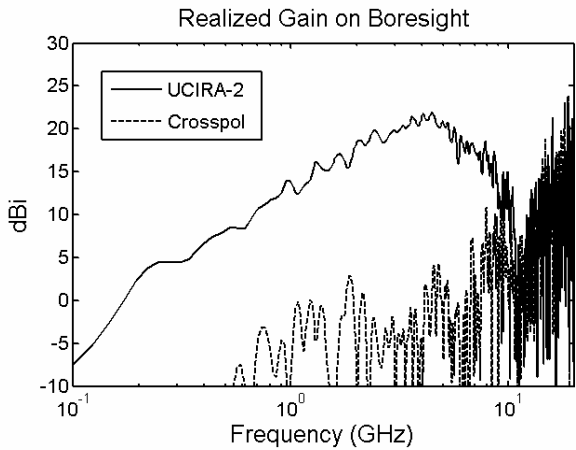


**Figure 6.4 Realized Gain of the UCIRA-2 in copol and crosspol configuration.**

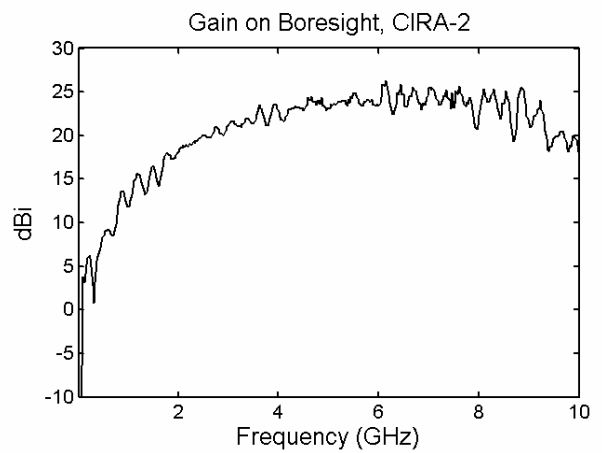
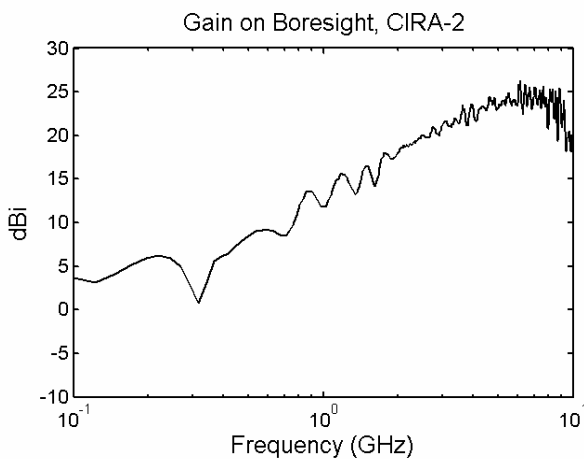


**Figure 6.5 Gain of the commercial CIRA-2.**

In Figure 6.7 and Figure 6.7 we show the antenna pattern of the UCIRA-2 on the major planes. The beamwidth is approximately 10-12°. The desired beamwidth is 20°, so it appears that we did not meet the goal; however, the shape of the antenna is not quite as accurate as we would like. The fabric reflector is approximately 4.3 cm (1.7 inches) deeper than desired and the distance from the feed point to the reflector is not as accurate as we would like. The reflector should be somewhat flatter than it is. This is in spite of several modifications that have improved the shape to some extent. It is very difficult to compensate for the stretch in the fabric and various effects of the sewing operation.

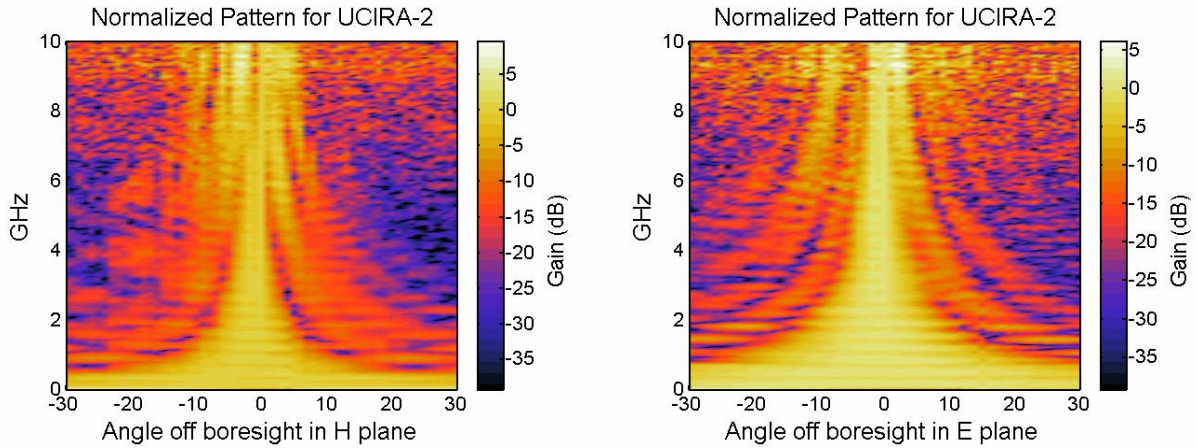


**Figure 6.6 Normalized antenna pattern in the H and E planes.**

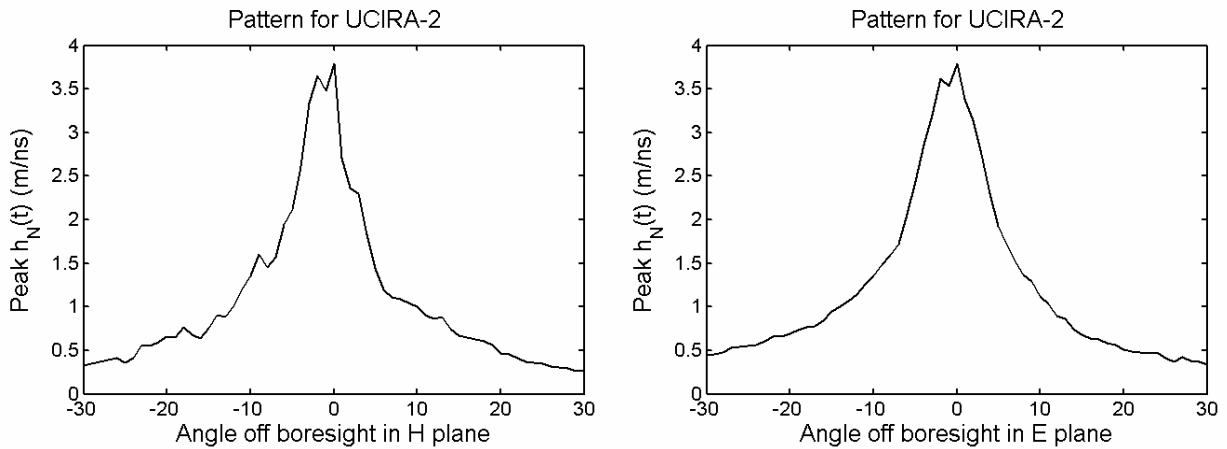


**Figure 6.7 Antenna pattern in the H and E planes based on peak impulse response,  $h_N(t)$ .**

## 7. UCIRA-2, RF Measurements in Dual Polarity Configuration.

Next, we provide the results of measurements made on the UCIRA-2 in dual polarity mode. First, we show the measurements for the feed arms in the vertical (V) plane and then the results for the arms in the horizontal (H) plane. In theory, the two should be identical. However, due to variations in the antenna especially at the feed point, the results are somewhat different. At the feed point, two of the wires from separate twinline feeds must cross to be connected to the tips of the feed arms in the proper configuration. This requires one wire to be in front of the other, so the wiring cannot be totally identical for the two feeds.

In Figure 7.1 we see that the impedance jumps at the feed point where the 200  $\Omega$  twinline connects to the 400  $\Omega$  feed arms. The impedance should jump from 50  $\Omega$  to 100  $\Omega$  in the TDR at this point due to the effect of the balun. However, in this case the jump is not that great. This is perhaps due to losses in the twinline that reduce the reflected voltage, so the full effect of the impedance mismatch is not seen in the TDR.

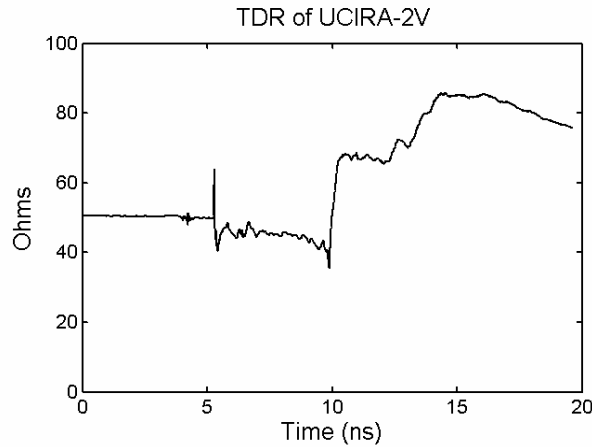


**Figure 7.1 TDR of the dual polar UCIRA-2 (Vertical).**

We present the impulse response for the vertical channel in Figure 7.2. The shape of the impulse response is not ideal and the FWHM is somewhat high. This leads to reduced gain at high frequencies as seen in Figure 7.3. In Figure 7.4 we show the theoretical gain for the UCIRA-2 in dual polarity mode based on work by J. Scott Tyo [3, 4]. The gain of the UCIRA-2 agrees reasonably well with the predictions, but it falls off more at 10 GHz. It is interesting that the reduced gain above about 5 GHz is due to defocusing the reflector, and not primarily due to antenna assembly problems as is sometimes the case.

One of our greatest challenges on this project has been the construction of the reflector so that it accurately maintains the desired hyperbolic shape. A considerable amount of dispersion results when the path lengths of various rays vary over the surface of the reflector. It is difficult to keep the weight of the antenna minimal, keep the force required to open the antenna reasonable and still have the stays strong enough to support the fabric reflector in the correct shape. It is also difficult to accurately sew the fabric. Other construction methods and materials may be available, but for this mechanical deployment scheme a very flexible material such as the

conductive rip-stop nylon is required. Thin plastic sheets would probably have a tendency to crack and/or tear during deployment or not lie flat after deployment.

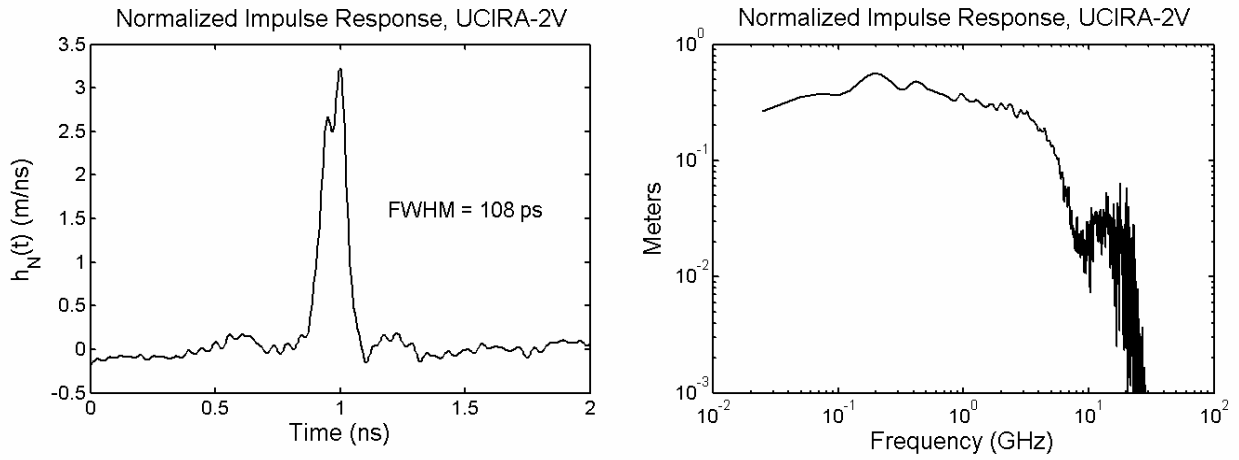


**Figure 7.2 Normalized impulse response.**

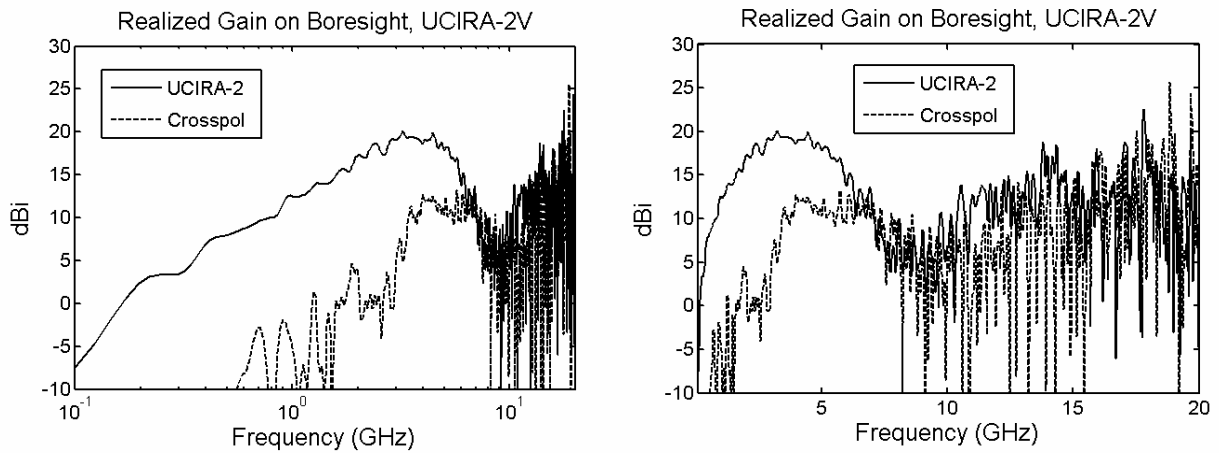


**Figure 7.3 Realized Gain of the dual polar UCIRA-2.**

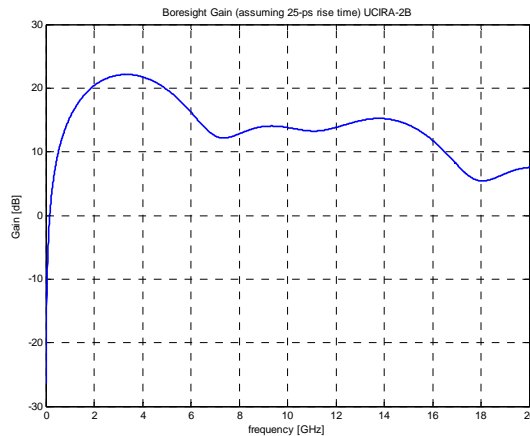


**Figure 7.4 Theoretical gain of UCIRA-2.**

We show the antenna patterns for the vertical channel in Figure 7.5 and Figure 7.6. The beamwidth in both planes is approximately  $12^\circ$ . This is approximately the same beamwidth obtained in the standard configuration (Figure 6.6 and Figure 6.7). This is not surprising since the reflector has not changed. As mentioned before, the design beamwidth was  $20^\circ$  so we are somewhat disappointed with this result.

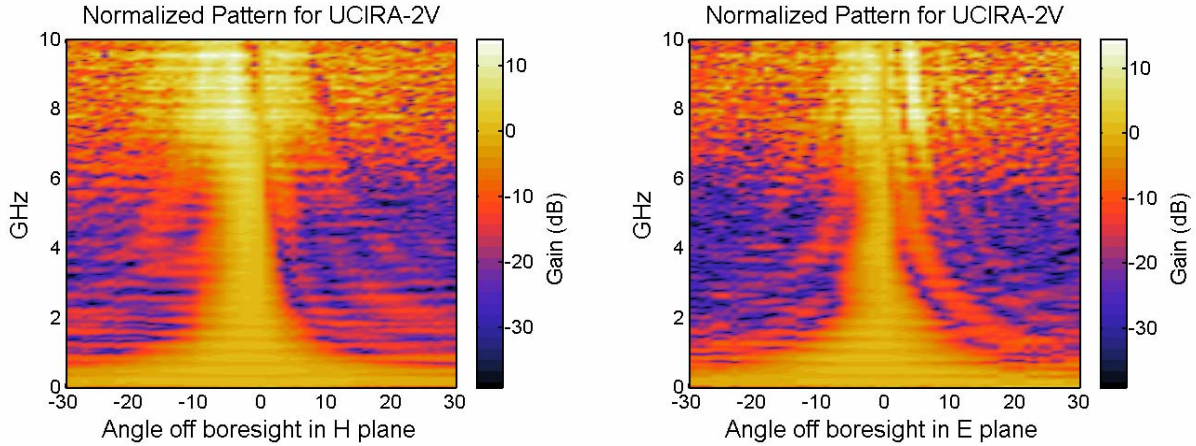


**Figure 7.5 Normalized antenna pattern in the H and E planes.**

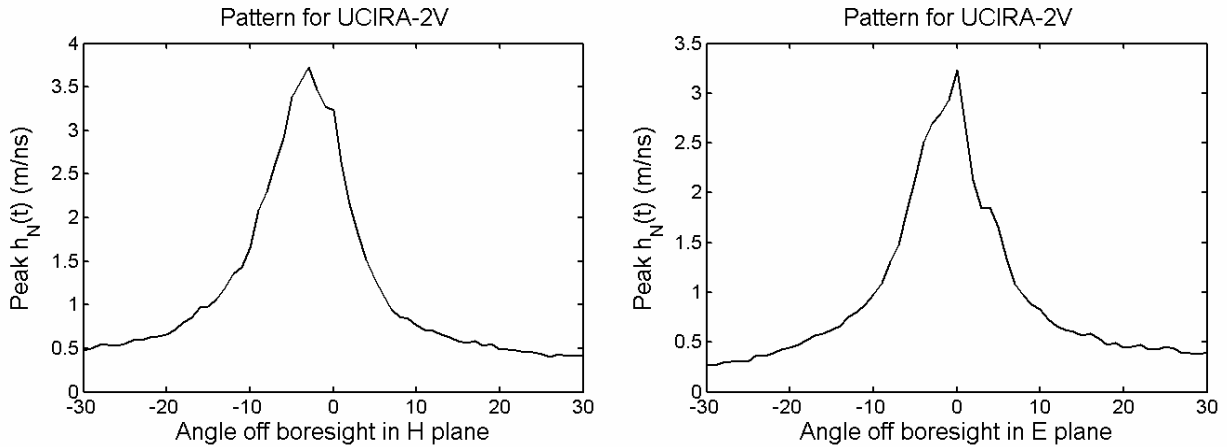


**Figure 7.6 Antenna pattern in the H and E planes based on the impulse response.**

We now show the results for the horizontal polarity. The TDR as shown in Figure 7.7 is about the same as in Figure 7.1.

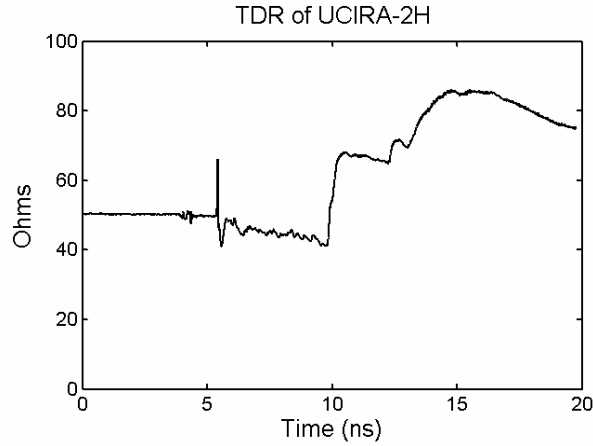


**Figure 7.7 TDR of the dual polar UCIRA-2 (Horizontal).**

The impulse response, shown in Figure 7.8, has the notch in a different place, which causes the FWHM to be much less. However, this is rather meaningless since the overall pulse is still quite wide and the response at high frequencies is still not as good as we might have hoped. By comparing Figure 7.3 and Figure 7.9 with Figure 6.4, we see that the gain of the antenna in the dual polarity mode is about 2-3 dB less than it is in the standard single feed mode. This relatively small loss, due largely to the impedance mismatch at the feed point, is a small price to pay for adding the dual polarity capability to the antenna.

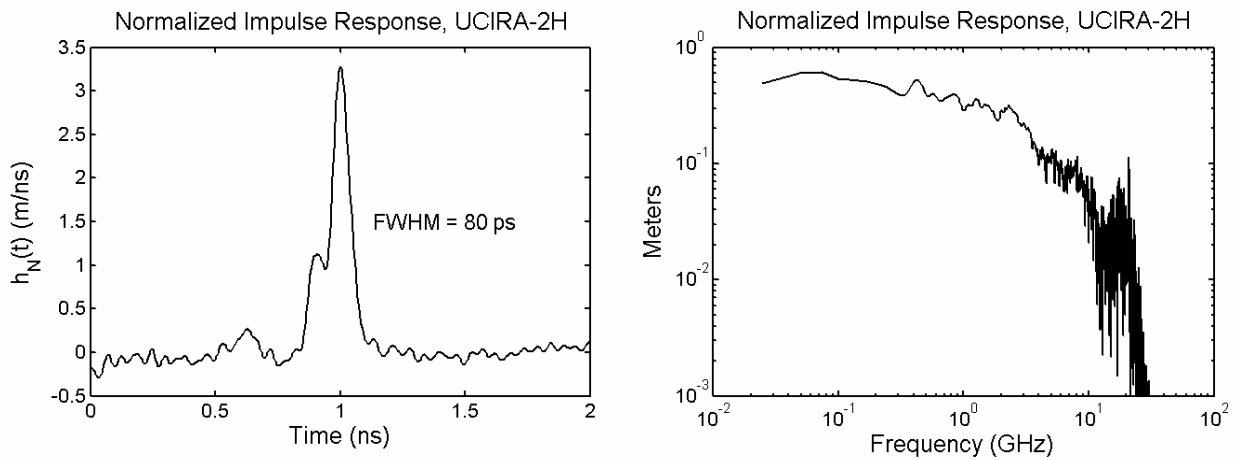


**Figure 7.8 Normalized impulse response.**

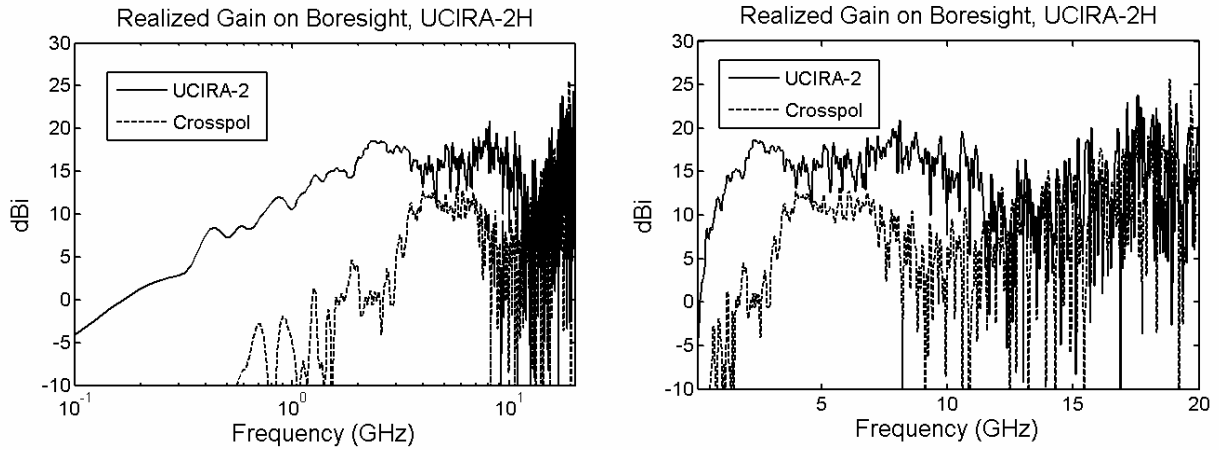


**Figure 7.9 Realized Gain of the dual polar UCIRA-2.**

In Figure 7.10 and Figure 7.11 we show the antenna patterns in this mode. The beamwidth is about  $12^\circ$  in the H plane and  $14^\circ$  in the E plane.

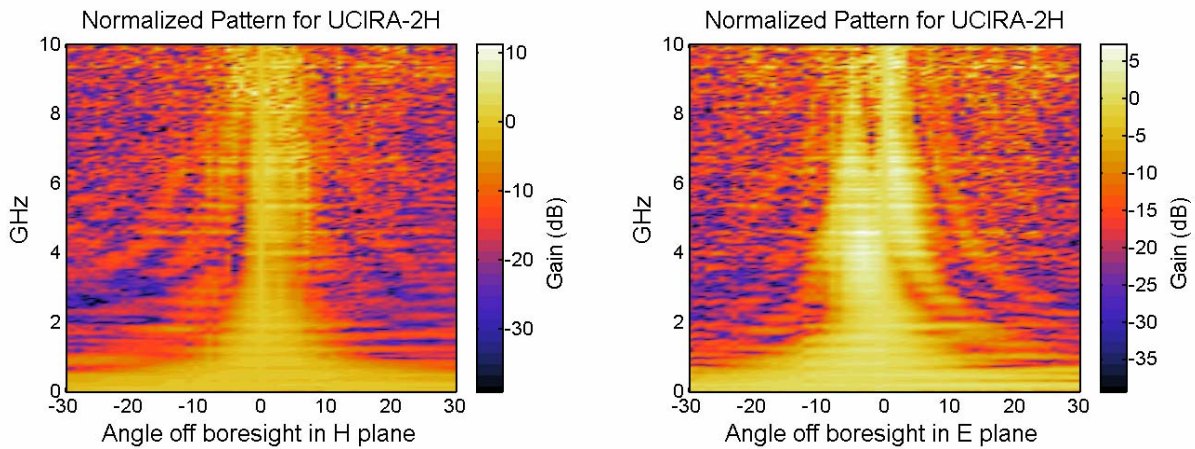


**Figure 7.10 Normalized antenna pattern in the H and E planes.**

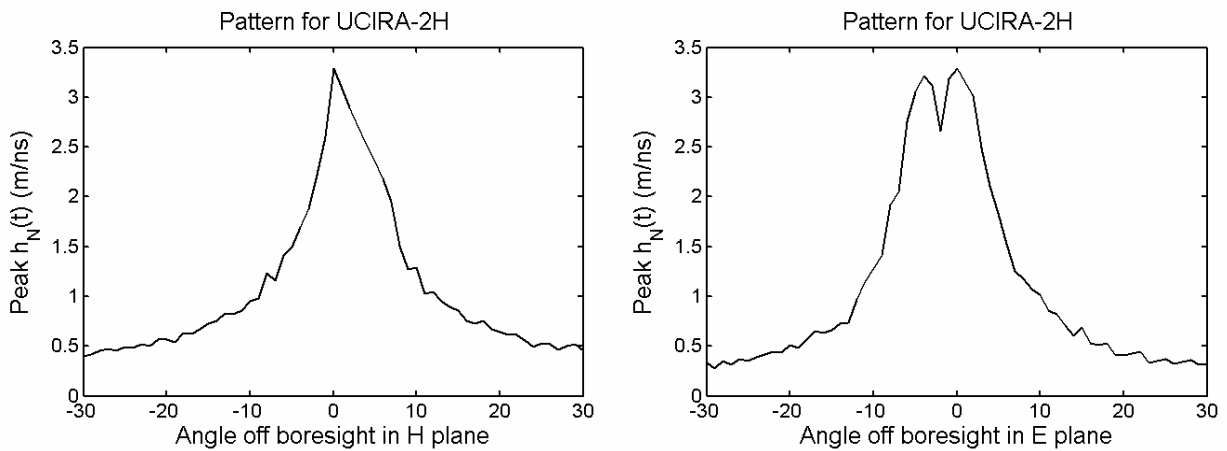


**Figure 7.11 Antenna pattern in the H and E planes based on the impulse response.**

## 8. UCIRA-2, Environmental Tests.

The UCIRA-2 was delivered to the Aerospace Engineering Facility (AEF) on Kirtland AFB on June 9, 2004 to begin the environmental tests. First the antenna was baked out in a small heated vacuum chamber to reduce or eliminate outgassing.

The test in the large Thermal/Vacuum (TVac) chamber was started on Monday June 14. The TVac chamber, as shown in Figure 8.1, is 2.13 m (84 inches) in diameter by 2.17 m (108 inches) in length. The UCIRA-2, in the stowed configuration, was placed in the chamber pointing vertically up. Four thermo-couples were attached to the body of the deployment mechanism to measure the temperature of the antenna. After the chamber was pumped down to approximately  $5 \times 10^{-5}$  Torr, the temperature was raised to +40°C for 1 hour. The temperature was then ramped down to -60°C. Before the temperature of the UCIRA-2 reached this temperature, however, the ERM released the cam so the antenna was in a partially deployed configuration with the antenna held closed by the band around the stays that must be released first for proper deployment. The pressure and temperature were then brought back to standard conditions, and the chamber was opened to determine the problem with the UCIRA-2.

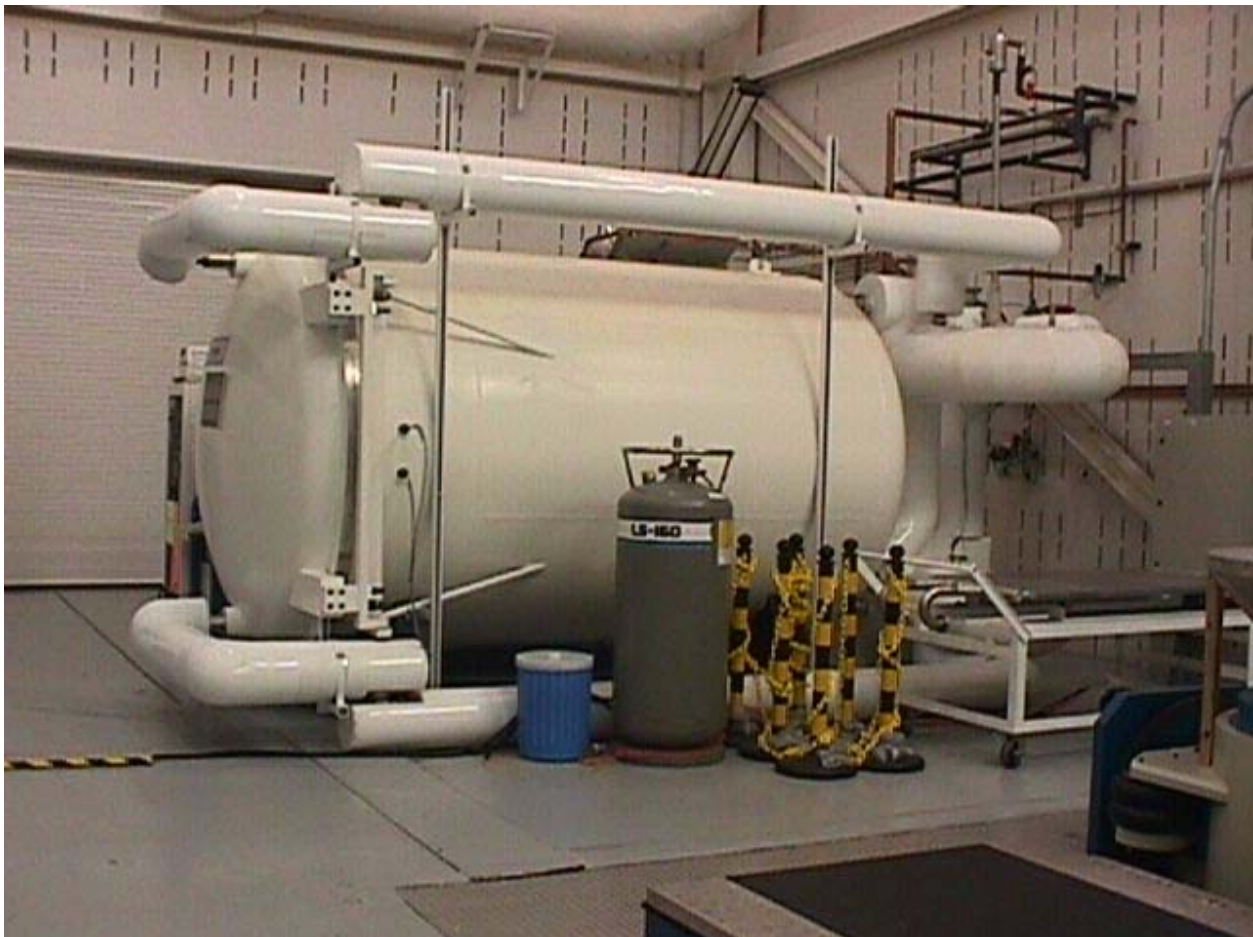


**Figure 8.1 Large Thermal Vacuum (TVac) Chamber.**

We tried to put the UCIRA-2 back in the stowed configuration but the ERM would not hold so we manually deployed the antenna and placed it back in the TVac chamber to continue the test. The UCIRA-2 in the deployed configuration is shown in Figure 8.2 mounted inside the TVac chamber. The chamber was then pumped down and the thermal cycling re-initialized. A video camera in the end of the chamber was used to photograph the antenna for 30 seconds every 30 minutes in an attempt to measure any deflection in the reflector. A grid was placed in the chamber near the rim of the reflector (card hanging in front of UCIRA-2) in hopes of being able to measure any deflection. This system did not function as well as hoped and the VCR attached to the camera was run at a slow speed which made viewing the tape on a standard VCR almost impossible. The lighting inside the chamber was also not very good. Viewing the video tape does; however, indicate that any deflection in the reflector was minimal.

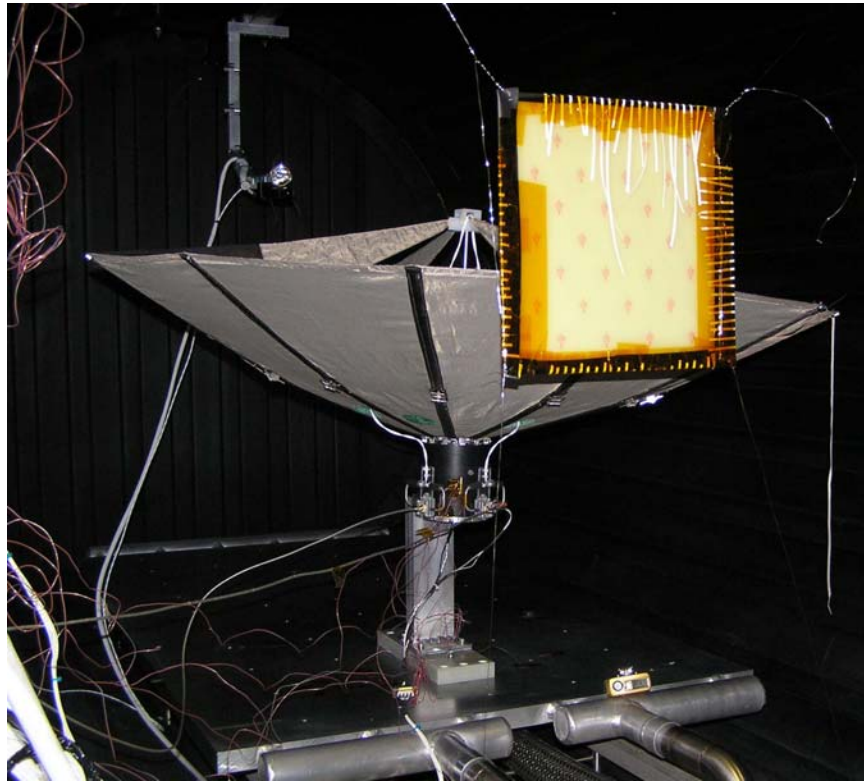


**Figure 8.2 UCIRA-2 mounted in TVac chamber.**

After the test, the ERM was returned to the manufacturer for repairs. The manufacturer reported that the wires that activate the device pushed against the internal mechanism in such a way as to simulate the release action of the device. The location where the wires exit the back of the ERM will need to be moved to prevent this in the future. The wires that activate the unit normally exit from the side, but for the UCIRA-2 they must exit through the rear.

The test in the TVac chamber was continued for 2 days. After the chamber was pumped down, the temperature was increased to  $+40^{\circ}\text{C}$  for 1 hour, which is the standard procedure to bake out any materials that might outgas. Then the temperature was reduced to  $-60^{\circ}\text{C}$  for 2 hours. The temperature was then increased to  $+70^{\circ}\text{C}$ , which is the maximum operating temperature for the ERM and pin puller and held for 2 hours. The chamber went through one

more complete thermal cycle before being returned to standard conditions and opened for removal of the UCIRA-2. The pressure during the thermal cycling varied from about  $2 \times 10^{-6}$  to  $3 \times 10^{-5}$  Torr.

In addition to taking video pictures of the antenna every 30 minutes, we also measured the TDR of one polarity of the antenna using a Tektronix TDS8000 with an 80E04 sampling head. Samples of the TDR measurements are shown in Figure 8.3. The TDR of the antenna does not change much with temperature, except at late time. Perhaps the resistance of the polypyrrole treated polyester used for the load resistors is temperature sensitive.

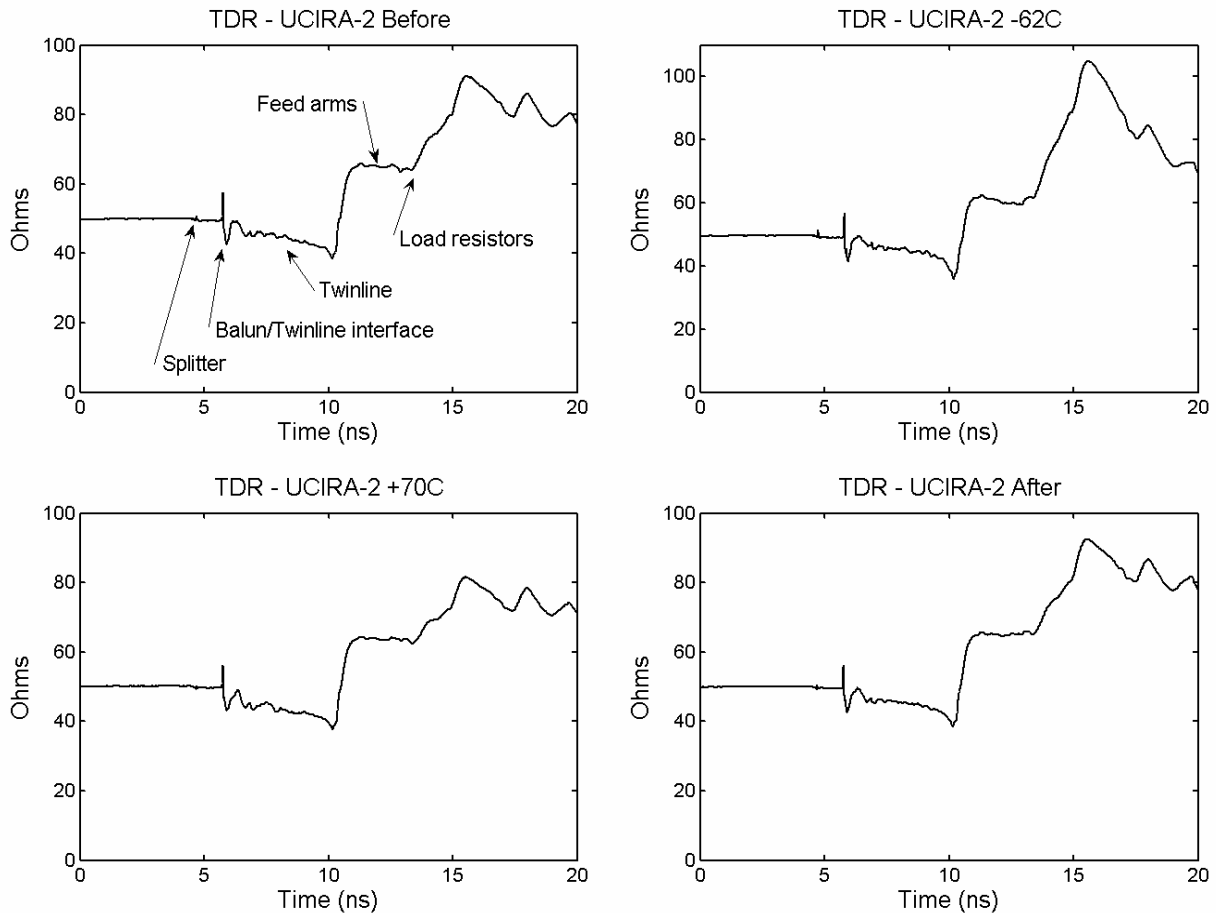


**Figure 8.3 TDR of UCIRA-2 in TVac chamber.**

We had planned to do full 3 dimensional vibration tests on the UCIRA-2; however, since we were not able to use the ERM to hold the cam in the stowed position, it was not possible to do the vibration tests. The vibration tests are only meaningful for the antenna in the stowed configuration, since that is the launch configuration. The vibration tests were to be done using both low level and high level sine sweeps. The low level sweeps were to determine resonant frequencies and the high level sweeps (or random vibration) were to determine launch survivability.

## 9. Conclusions and Recommendations

We built three versions of the Ultra-Compact Impulse Radiating Antenna, or UCIRA, which was intended for space applications. The first version, the UCIRA-1, had electrical performance that was only slightly less than that of our commercial CIRA-2. This was a remarkable result, because the UCIRA-2 had a twinline feed instead of the coaxial cable feed in the CIRA-2. In its collapsed position, the UCIRA-1 was smaller than our commercial CIRA, but a manual operation was required to deploy it. In the UCIRA-1B, we attempted to improve the boresight gain by removing the negatively contributing portion of the reflector. This resulted in performance that was less than that of the UCIRA-1, because the reflector shape came out worse than before.

In the final version of the UCIRA, the UCIRA-2, we introduced a number of improvements. We incorporated an automatic deployment mechanism, we defocused the aperture to broaden the beam, we allowed for dual polarization, and we used materials that could be qualified for space operation. Since the feed arms were positioned at equal 90-degree increments around the edge of the reflector, we could feed the antenna either as a single-polarization antenna with good impedance match, or as a dual polarization, dual channel antenna with a 2:1 impedance mismatch. When configured as a single-polarization antenna, the gain was considerably less than that of our commercial CIRA-2, because the reflector was defocused into a hyperboloid. When configured as a dual channel antenna, each channel performed well only up to 4-5 GHz, which is sufficient for many applications.

After studying the various materials that could be used in space applications, the materials used in the UCIRA-2 were very similar to or the same as those used for earlier collapsible antennas. We found a better conductive fabric for the reflector, and we found that nylon should be a satisfactory fabric for this application. The Tuftram® surface treatment on the aluminum was a big improvement. This process forms a heavy aluminum oxide coating on the aluminum and then a polymer is infused into the surface to form a self-lubricating surface.

The development of the balun/twinline feed was a major success, since the feed for a deployable antenna must be very flexible. The attenuation measured for this type of feed was low enough over the frequencies of interest that it could be used for the satellite application considered here.

Because of a bug in our ERM, we were able to complete only a portion of the environmental testing. A slight modification to the ERM actuator will make it possible to complete the testing should the need arise later.

There are several minor mechanical modifications that will improve the deployment of the reflector. Using composite rods for the stays with a slightly larger diameter should stretch the reflector tighter to obtain a better shape. Longer stay adapters should be used to reduce the forces on the ends of the stays. A method of fabricating the reflector other than sewing may provide a more accurate reflector.

## Appendix A. Defocusing a Paraboloid into a Hyperboloid

In order to broaden the beamwidth of the UCIRA, we defocus the aperture by converting the paraboloidal reflector into a hyperboloid. In doing so, we must maintain the same reflector diameter and focal length. We specify an angle,  $\phi_o$ , which is the angle at which the extreme ray at the edge of the reflector deviates from the focal direction, as shown in Figure A.1. When  $\phi_o = 0$ , the hyperboloid reverts back to the paraboloid.

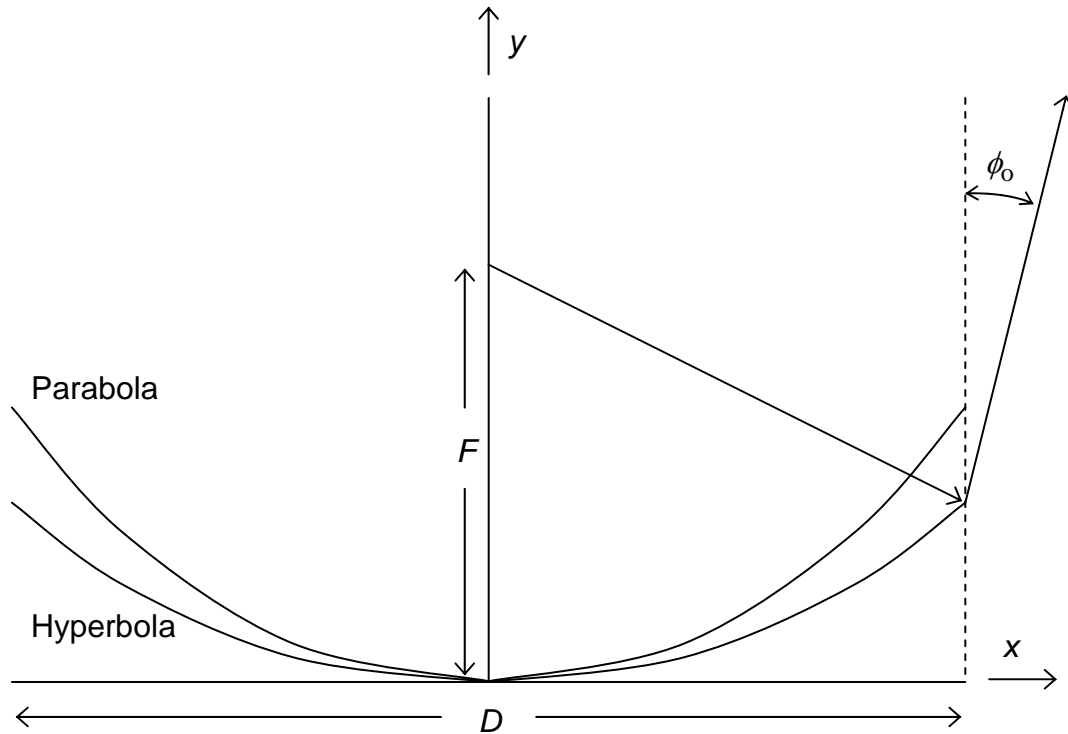


**Figure A.1** The conversion of a paraboloidal reflector to a hyperboloidal reflector.

It is unclear how the parameter  $\phi_o$  affects the beamwidth. At extremely high frequencies, the beamwidth is  $2\phi_o$ , which is the optical limit. In practice, of course, this is never achieved. As proof of this, a focused paraboloid with  $\phi_o = 0$  does not have a beamwidth of  $0^\circ$  at any frequency. At lower frequencies, a reasonable guess is that the beamwidth will broaden the beamwidth by an extra  $2\phi_o$  beyond the beamwidth of the focused (paraboloidal) case. J. Scott Tyo has investigated this in somewhat more detail in [4]

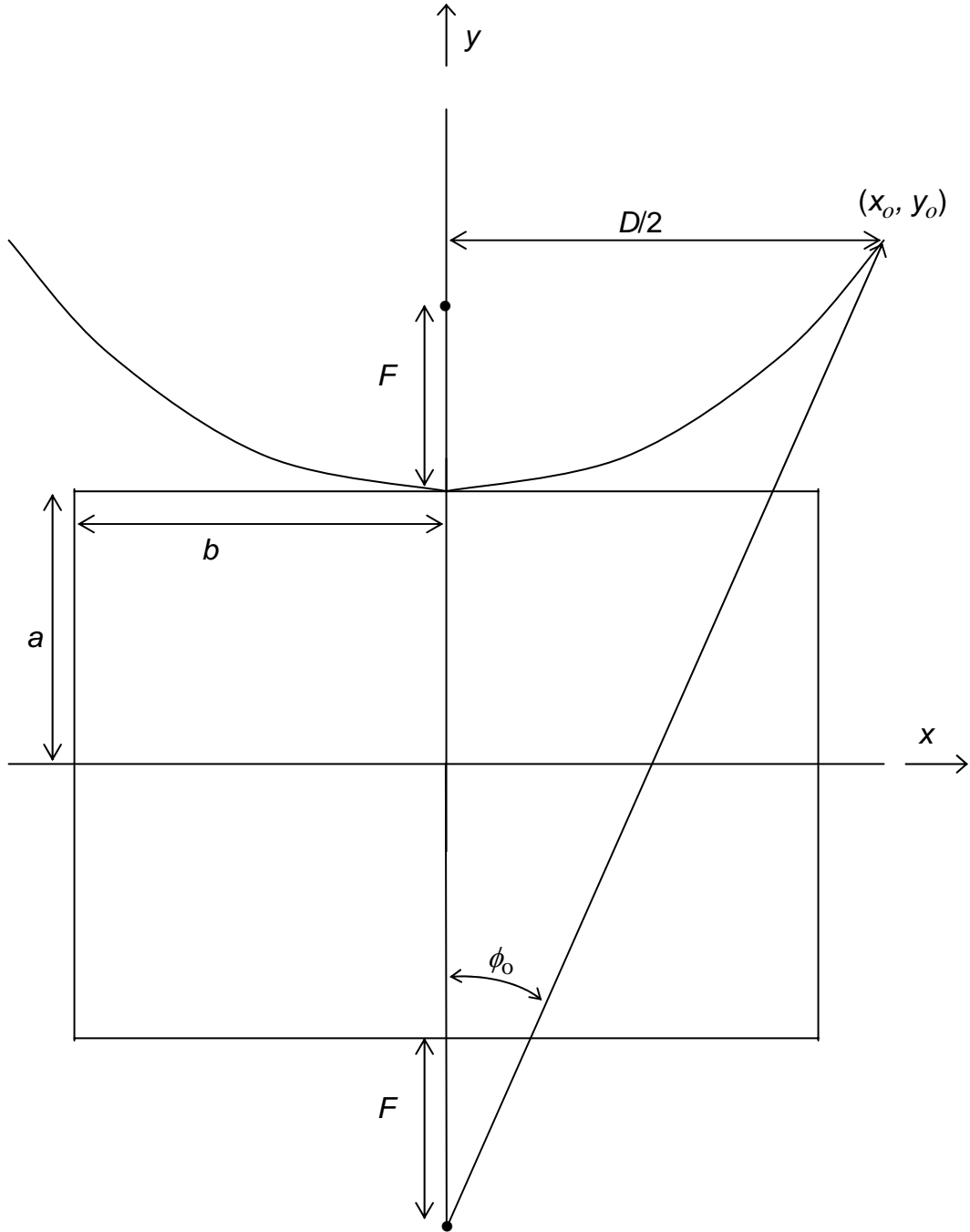


**Figure A.2 Geometry of the hyperbola.**

We calculate now the relationship between the parabola and hyperbola. The equation of the parabola in Figure A.1 is

$$y = \frac{1}{4F} x^2 \quad (\text{A.1})$$

The equation of the hyperbola in Figure A.2 is

$$\frac{y^2}{a^2} - \frac{x^2}{b^2} = 1 \quad , \quad y = a\sqrt{1 + \frac{x^2}{b^2}} \quad (\text{A.2})$$

where  $a$  and  $b$  are the dimensions of the box that determine the asymptotes of the hyperbola. To get the hyperbola to intersect the origin as does the parabola in Figure A.1, we will have to shift the hyperbola down by a distance  $a$ . We postpone this until the end of the derivation in order to simplify the math.

We now solve for the hyperbola that has the specified  $F$ ,  $D$ , and  $\phi_o$ . From the basic properties of the hyperbola we have [16]

$$\begin{aligned} c &= a + F \\ c^2 &= a^2 + b^2 \\ b^2 &= c^2 - a^2 = F(2a + F) \end{aligned} \quad (\text{A.3})$$

so the equation for the hyperbola becomes

$$\frac{y^2}{a^2} - \frac{x^2}{F(2a + F)} = 1 \quad (\text{A.4})$$

From Figure A.2 we see

$$\tan(\phi_o) = \frac{D/2}{y_o + c} \quad (\text{A.5})$$

where  $(x_o, y_o)$  denotes the edge are the coordinates of the intersection of the extreme ray with the hyperbola. Note that after reflection the extreme ray originates at the second focus of the hyperbola. To find the intersection of the extreme ray with the edge of the hyperbola, we use equation (A.4) at  $x_o = D/2$  to find

$$y_o = a\sqrt{1 + \frac{(D/2)^2}{F(2a + F)}} \quad (\text{A.6})$$

We now combine the above two equations and identify a parameter  $q = \tan(\phi_o)$  to find

$$q = \frac{D/2}{a\sqrt{1 + \frac{(D/2)^2}{F(2a+F)}} + a + F} \quad (\text{A.7})$$

The only unknown in this equation is  $a$ . This can be expanded and simplified, after which we are left with a quadratic equation in  $a$  to solve,

$$\left(q^2(D/2)^2 + 4Fqw\right)a^2 + \left(2qwF^2 - 2Fw^2\right)a - F^2w^2 = 0 \quad (\text{A.8})$$

where  $w = D/2 - qF$ . This is solved in the usual manner, keeping in mind that we obtain two values for  $a$ , and that a negative value is nonphysical. Only one of the two solutions will satisfy equation (A.5), so that is the correct solution. Once we have solved for  $a$ , we find  $b$  and  $c$  from equation (A.3). This completely specifies the hyperbola, however it intersects the  $y$ -axis at  $y=a$ . To get the hyperbola to intersect the origin as shown in Figure A.1, we need to shift it down by a distance of  $a$ .

As an example, we consider a reflector 1.22 meters (4 feet) in diameter, with  $F/D = 0.3$  and  $\phi_o = 10$  degrees. Both the original parabola and the hyperbola are shown in Figure A.3.

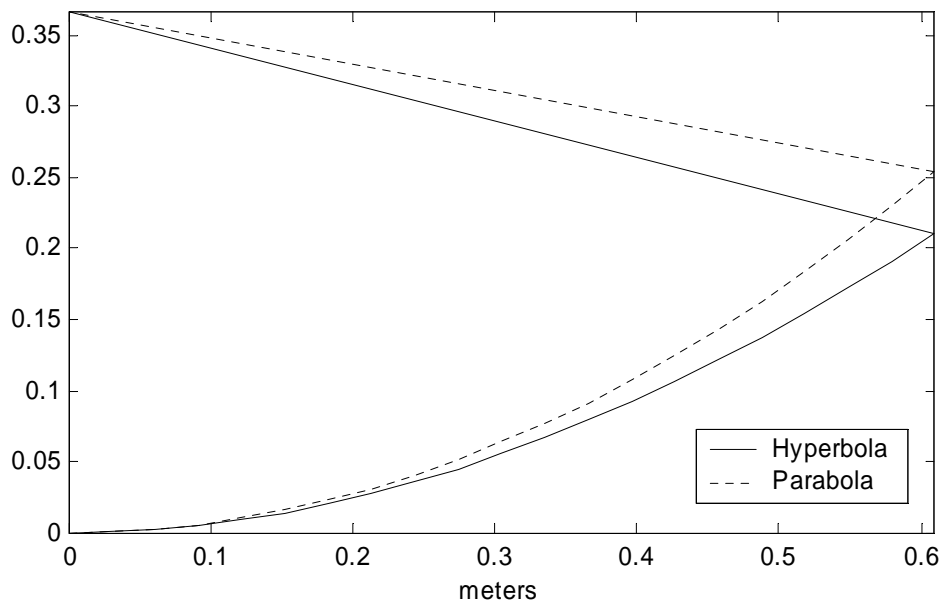


**Figure A.3** Example of defocusing a parabola into a hyperbola with  $F/D = 0.3$  and with a defocus parameter of  $\phi_o = 10^\circ$ .

## References.

---

- 1 L. H. Bowen, E. G. Farr, J. P. Paxton, A. J. Witzig, C. E. Baum, D. I. Lawry, and W. D. Prather, "Fabrication and Testing of a Membrane IRA", Sensor and Simulation Note 464, January 2002.
- 2 L. H. Bowen, E. G. Farr, and W. D. Prather, "An Improved Collapsible Impulse Radiating Antenna," Sensor and Simulation Note 444, April 2000.
- 3 J. S. Tyo, E. G. Farr, L. H. Bowen, J. S. H. Schoenberg, "Off-boresight radiation from impulse radiating antennas," Antennas and Propagation Society International Symposium, 2003. IEEE, Volume: 1, 22-27, June 2003.
- 4 J. S. Tyo, E. G. Farr, and D. I. Lawry, "Effect of Defocusing on the Prompt Response of an IRA: I. Hyperbolic Reflector," Sensor and Simulation Note 486, November 2003.
- 5 L. H. Bowen, E. G. Farr, C. E. Baum, T. C. Tran, and W. D. Prather, "Experimental Results of Optimizing the Location of Feed Arms in a Collapsible IRA and a Solid IRA," Sensor and Simulation Note 450, November 2000.
- 6 C. E. Baum, Aperture-Antenna Synthesis for Hyperband SAR Antennas, Sensor and Simulation Note 466, February 2002.
- 7 L. H. Bowen, E. G. Farr, and D. I. Lawry, "A Dual-Polarity Impulse Radiating Antenna," Sensor and Simulation Note 479, October 2003.
- 8 L. H. Bowen, E. G. Farr, C. E. Baum, and T. C. Tran, "Optimization of Impulse Radiating Antennas," in Mokole *et al* (eds.), *Ultra-Wideband Short-Pulse Electromagnetics 6*, New York, Kluwer Academic/Plenum Publishers, 2003.
- 9 J. S. Tyo, "Optimization of the Feed Impedance for an Arbitrary Crossed-Feed-Arm Impulse Radiating Antenna," Sensor and Simulation Note 438, November 1999.
- 10 J. S. Tyo, "Optimization of the TEM feed structure for four-arm reflector impulse radiating antennas," *IEEE Trans. Antennas and Propagation*, Volume: 49, Issue: 4, April 2001.
- 11 L. H. Bowen, E. G. Farr, C. E. Baum, T. C. Tran, and W. D. Prather, "Results of Optimization Experiments on a Solid Reflector IRA," Sensor and Simulation Note 463, January 2002.
- 12 J. S. Tyo, E. G. Farr, J. S. H. Schoenberg, L. H. Bowen, L. L. Altgilbers, "Effect of Aperture Feed and Reflector Configuration on the Time- and Frequency Domain Radiation Patterns of Reflector Impulse Radiating Antennas," *IEEE Trans. Antennas and Propagation*, Volume: 52, Issue: 7, July 2004.
- 13 J. S. Tyo, "IRA Variations Useful for Flexible Feed Arms," Sensor and Simulation Note 472, March 2003.

- 
- 14 M. J. Baretela, J. S. Tyo, "Improvement of prompt response from impulse radiating antennas by aperture trimming," IEEE Transactions on Antennas and Propagation, Volume: 51, Issue: 9, September 2003.
  - 15 R. L. Fusaro, Ed. "NASA Space Mechanisms Handbook and Reference Guide," NASA/TP-1999-206988, July 1999.
  - 16 G. B. Thomas, *Calculus and Analytic Geometry*, Alternate Edition, New York, Addison Wesley, 1972, pp. 494-498.